CrossMark

RESEARCH ARTICLE

Neural network modelling of the influence of channelopathies on reflex visual attention

Alexandre Gravier[1] · Chai Quek[2] · Włodzisław Duch[3] · Abdul Wahab[4] ·
Joanna Gravier-Rymaszewska[5]

Abstract This paper introduces a model of Emergent Visual Attention in presence of calcium channelopathy (EVAC). By modelling channelopathy, EVAC constitutes an effort towards identifying the possible causes of autism. The network structure embodies the dual pathways model of cortical processing of visual input, with reflex attention as an emergent property of neural interactions. EVAC extends existing work by introducing attention shift in a larger-scale network and applying a phenomenological model of channelopathy. In presence of a distractor, the channelopathic network's rate of failure to shift attention is lower than the control network's, but overall, the control network exhibits a lower classification error rate. The simulation results also show differences in task-relative reaction times between control and channelopathic networks. The attention shift timings inferred from the model are consistent with studies of attention shift in autistic children.

✉ Alexandre Gravier
   al0001er@e.ntu.edu.sg

1 Centre for Computational Intelligence (C2i), Nanyang Technological University, N4-B1A-02, Nanyang Avenue, 639798 Singapore, Singapore

2 School of Computer Engineering, Nanyang Technological University, Singapore, Singapore

3 Department of Informatics, School of Physics, Astronomy and Informatics, Nicolaus Copernicus University, Torun, Poland

4 School of Information and Communication Technology, International Islamic University of Malaysia, Kuala Lumpur, Malaysia

5 School of Humanities and Social Sciences, Nanyang Technological University, Singapore, Singapore

Introduction

The computational modelling approach is a relative new-comer to neuroscientific enquiry, but can be a valuable tool to generate hypothesis and complement the experimental methods used in more traditional sciences of behaviour and cognition. In particular it may be useful to study the effects of channelopathies, dysfunctions of ion channels, on cognitive functions. In this paper some aspects of the brain-to-behaviour links are investigated. Defects to L-type voltage-gated calcium channels (LTCC) are hypothesised to play a role in certain cases of autism. A novel neural network model of the influence of calcium channelopathy on bottom-up visual attention (EVAC) is developed.

Autism is a pervasive developmental disorder of unknown etiology which affects several aspects of the behaviour, and is defined by a set of core symptoms. These symptoms are highly heterogeneous, therefore the term Autism Spectrum Disorder (ASD) is commonly used. Because understanding ASD is a difficult scientific problem with important human and societal repercussions it has been studied using a large spectrum of approaches (Zimmerman 2008). Autism was studied from many perspectives: molecular and clinical genetics, neurotransmitters and cell signaling, endocrinology, growth, and metabolic processes; immunology, maternal-fetal effects, and neuroinflammation, environmental influences, neuroanatomy, brain imaging, and neural networks. While great efforts have been devoted to genetics of ASD it is clear now that hundreds of genes are involved affecting the neuroskeleton and synapses (Michael et al. 2014). Genetics by itself can

tell us only about neural structures that are broken, but will not elucidate the mechanisms that lead to mental disfunctions. Therefore in this paper the neurodynamical perspective is investigated (Duch et al. 2013; Duch and Dobosz 2011; Dobosz and Duch 2010).

At the neurological end of the spectrum, neuroimaging techniques still lack in either temporal or spatial resolution. Hence, detailed observations of neural dynamics sufficiently large in scale to unambiguously solve the problem of autism causation can not be obtained. At the other, more theoretical end, psycho-developmental theories of autism, while intellectually attractive and elegantly designed to fit existing frameworks, are not validated, for want of substantiating clinical observations. Computational modelling has the potential to help the study of autism by filling the gap between descriptive neuroscience and more abstract psychology models. Explanations at the level of neurodynamics may be linked to specific biophysical properties of neurons resulting from protein and genetic abnormalities, and may show how neurodynamical states of network composed of such neurons lead to a specific cognitive, emotional and behavioral dysfunctions. To achieve this goal models of neurons should be sufficiently detailed to distinguish, at least in a coarse way, between different types of ion channels. Neural models of ASD that provide only general sweeping view of neural dynamics may still be useful but cannot be linked to experimental neuroscience (Grossberg and Seidman 2006). In contrast, existing computational studies of low-level neuronal mechanisms have demonstrated that accurate modelling of neuronal response can lead to biologically realistic systemic behaviours (Lanyon and Denham 2009).

The theory of autism causation is presented here in the context of a computational model of bottom-up visual attention derived from O'Reilly and Munakata (2000). It aims at formulating a preliminary model of how autism calcium channelopathy (Piedras-Rentería et al. 2007) can lead to the disturbed attentional mechanisms observed in some cases of ASD (Courchesne et al. 1994; Townsend et al. 1996; Geest et al. 2001). While neither the mechanistic model of bottom-up attention used here (O'Reilly and Munakata 2000), nor the channelopathy hypothesised to be at the origin of some cases of autism spectrum disorders are novel (Duch et al. 2013; Dobosz and Duch 2010; Wany and Wojcik 2014), their simulation and integration into the model of emergent visual attention with channelopathy (EVAC) are new.

The EVAC model is a recurrent neural network that implements the dual-pathway model of vision. In this model, information from the retinas is first transformed by a common processing pipeline of sub-cortical and cortical maps (retina, LGN and V1 area), and later processed by several cortical layers in two separate streams,

parietal and inferotemporal. The synaptic weights of the artificial neural network must be trained to learn the correct input-output associations, requiring recognition of the spatial position and the type of object. In EVAC, the majority of the learning is done using the Leabra learning algorithm (O'Reilly and Munakata 2000; Aisa et al. 2008).

Besides the trained dual-pathway network, EVAC also embodies the emergent theory of bottom-up visual attention, which was first modelled computationally by O'Reilly and Munakata (2000). In this theory, a shift of attention to a new salient stimulus is not the result of the activation of a unique saliency map, but an emergent property of the network that results from the *accommodation* property of individual neural units. Neuronal accommodation mechanism apprehend the decreasing response of neurons to input after sustained activity. This phenomenon is mediated by several processes, but mostly depends on the short-term history of activity of the neuron, and the dynamics of spontaneous depolarisation, affected by channelopathy. Thus, it is expected that channelopathy affects reflex visual attention. The model developed does not account for top-down attention (see e.g. (Gu and Liljenstrm 2007) for a computational model that includes prefrontal influence). This is in part justified by the short timescale involved in reflex visual attention.

The model of EVAC is instantiated with two different parameter sets, resulting in: (1) a control network designed to model attention shift of neurotypical subjects, and (2) a channelopathic network that aims at modelling the attention shift in subjects suffering from calcium channelopathy. The trained networks are tested on attention shift tasks in the framework of the well-known Posner visual orientation task (Posner 1980).

The change of activations of all layers partly mediated by accommodation is observed to result in attention shift with significantly different timings depending on the presence of channelopathy. The error rates also vary, but to a lesser extent. The simplifications made in designing the network model do not allow for a direct translation of simulated time units to real time. However, the relative time differences between the channelopathic network and the control network are expected to be qualitatively comparable to the clinical trials on Posner-type orientation task. Hence, the results of the simulation of the control and channelopathic EVAC networks on three attention shift tasks results in several testable predictions about the relative attention shift performance of subjects suffering from channelopathy compared to controls. As it is plausible that channelopathy explains certain cases of autism, these simulation results are compared to existing studies of reflex attention in autistic children, showing concordance with experimental results.

Materials and methods

The structure of the EVAC model is specified by defining:

- cognitive function,
- structure of neurons,
- network architecture—connectivity and learning, and
- the model of channelopathy.

Here both the network model, and the cognitive function simulated, are inspired by the computational studies of O'Reilly and Munakata (2000). While Emergent does not allow for detailed structure of individual neurons Bower and Beeman (1998) it is easier to use in a large-scale simulations providing insight into the mechanisms involved Aisa et al. (2008). Simulations of cognitive functions follow the Posner visual orientation task (Posner 1980).

The EVAC model uses eight layers of neurons to implement the dual-pathway visual system. The Hodgkin-Huxley type point neurons (Hodgkin and Huxley 1952) that populate these layers connect bidirectionally adjacent layers by excitatory projections, while inhibition within each layer ensures that activity is sparse, simulating winner-takes-all dynamics of cortical minicolumns.

The synaptic weights are learnt using a hybrid self-organised and error-driven algorithm called Leabra, introduced by O'Reilly in (O'Reilly 1996b). This algorithm tries to approximate biologically realistic network dynamics using distributed representations, inhibitory competition, bidirectional activation propagation, Hebbian competitive learning similar to Kohonen maps (Kohonen 1982) with the error-driven learning principles based on the Generalised Recirculation algorithm (O'Reilly 1996a). The model is implemented in the Emergent simulation environment (O'Reilly and Munakata 2000; Aisa et al. 2008).

Relations between mutations of specific genes that have strong expression in occipital lobe (such as MET, KCNS1, NRXN1, SLC6A10P, NPY1R genes) has been noted in (Duch et al. 2013). These genes influence neural circuits relevant to the emergent synchronization necessary for processing of complex visual stimuli, including faces. In particular mutations of the KCNS family of genes involved in forming leak ion channels (the two-pore delayed-rectifier potassium voltage-gated ion channels), contribute to the spontaneous depolarization of neurons. This is captured in our model by quantitative changes to parameters controlling the dynamics of the response of neurons to their polarization on different timescales. Such accommodation or neural fatigue may slow down attentions shifts of attention (ASD case) or prevent longer focus (ADHD case). Many types of channelopathies may have similar influence on neural dynamics, leading to a great heterogeneity of symptoms in autism spectrum disorder and other

attention-related disorders. In particular the role of calcium signaling abnormalities, linked to the L-type voltage-gated calcium channelopathies, has been documented in the literature (McEnery et al. 1998; Gargus 2009; Splawski et al. 2004; Krey and Dolmetsch 2007). This hypothesis of the etiology of ASD and other disorders is modelled at the neural network level changing the biophysical properties of neurons to reflect influence of channelopathies on neural dynamics.

Psychological tasks models

The aim is to model human visual attention capture and measure its timing in a neuron-level simulation. For that, we design several input/output tasks that the network then performs repeatedly to collect timing and performance statistics. These tasks are inspired by existing studies in psychology and computational cognitive neuroscience (O'Reilly and Munakata 2000; Posner 1980).

The attention experiment in (O'Reilly and Munakata 2000, p. 261) uses the simplest possible model of visual processing[1] to qualitatively illustrate that the timing differences between valid and invalid trials are compatible with bottom-up, emergent visual attention.

O'Reilly and Munakata also attempted to implement a spatial attention shift model (O'Reilly and Munakata 2000) using the PDP++ simulator, without success.[2] Structurally, the EVAC model of reflex visual attention is improving on and implementing the attention shift model by O'Reilly and Munakata (2000) in Emergent. The tasks are inspired by the Posner paradigm (Posner 1980).

The Posner paradigm originally aimed at assessing the influence of the covert orienting of attention on reaction time in a simple task: the subject is first shown a visual cue, followed by an off-centre stimulus. The cue may indicate where to expect the stimulus to appear (this is called a valid trial), or may be misleading (in an invalid trial). Posner considers variations of in the timing between the appearance of the second stimulus and the saccade towards it in terms of of three phases: *disengaging* from the current focus of attention, *moving* attention to the location of the target, and *engaging* the target.

Our computational experiment comprises of three simple task conditions: Neutral, Gap, and Overlap. Like in the Posner paradigm, these tasks allow the exploration of the way interaction between the ventral and dorsal processing streams enable the reflex orientation of attention. Each task

---

[1] The model in (O'Reilly and Munakata 2000) uses a one-dimensional input space comprising of 7 discrete locations, 2 input categories input on a 14-units map diverging into a dorsal and a ventral pathway, each comprising of one hidden and one output layer.

[2] See authors' note at grey.colourado.edu/CompCogNeuro.

corresponds to one condition, and is either performed by a network with units simulating channelopathy, or by a control network, with nominal unit parameters.

The Neutral condition

The Neutral condition is meant to assess the time to fix attention in the absence of any distractor, from a neutral state of activity.

In this condition, the network is at rest, without any input stimulus. After a short period of time, a stimulus appears at a random location on the input map. The time is measured from the appearance of that stimulus to the settling of the dorsal and ventral maps on the correct location and identity. Figure 1 is a time diagram of the Neutral task condition, showing its two phases $N(1)$ and $N(2)$.

The Neutral condition is a control condition, as it is not an attention shift task, but meant to be compared against the other conditions that are directly related to attention shift. In terms of the three phases of attention shift that were posited by Posner, the Neutral condition should assess the time to *move* attention to the location of the target, and to *engage* the target. The *disengagement* from the current focus of attention does not exist in the Neutral condition, because the network is not presented with any input.

At the start of the task, the network activity is null, and all neurons' membrane potentials are at rest. Hence, it is expected that, during the first phase of the Neutral task condition $N(1)$, in which there is no input, the output layers of the control network remain inactive. The channelopathic network should also remain inactive, as accommodation and hysteresis, the two parameters affected by channelopathy, only affect the activity of neurons beyond a short period of activity. During the second phase of the

Neural task condition $N(2)$, the timing engagement of attention to the emerging stimulus could be affected by channelopathy. The task finishes when both output maps have settled on the correct stimulus location and identity, or failed to do so after a timeout.

The movement of attention is a psychological concept that is expected not to have a great significance at the neural level in the Neutral task, as attention is not shifted from one location to another, or from one object identity to another. Instead, activity is expected to emerge at the right spatial location on the dorsal output map, and with the correct output category, thanks to the interaction of all maps' k-WTA inhibition and bidirectional excitation.

The Gap condition

The Gap condition is the first of the attention shift tasks. It is meant to study attention shift when the network has recently been (but is not anymore) presented with a distractor.

The four phases of the timeline of the Gap condition are represented in Fig. 2. During phase $G(1)$, the network is first run without any stimulus for a small duration. Afterwards, the input sequence is divided in three phases. First, during phase $G(2)$, a stimulus is presented to the input map in a random location A. After a while, this stimulus disappears, and the input map remains turned off for a fixed duration [phase $G(3)$]. Finally, during phase $G(4)$, a new stimulus appears at a location $B \neq A$ and remains displayed on the input map until both output maps show the correct stimulus location and identity, or a timeout is reached. The duration of phase $G(4)$ during a successful trial determines the speed of attention shift to the stimulus at location B.

Fig. 1 Organisation of the Neutral task condition in the simulated reflex attention shift experiment
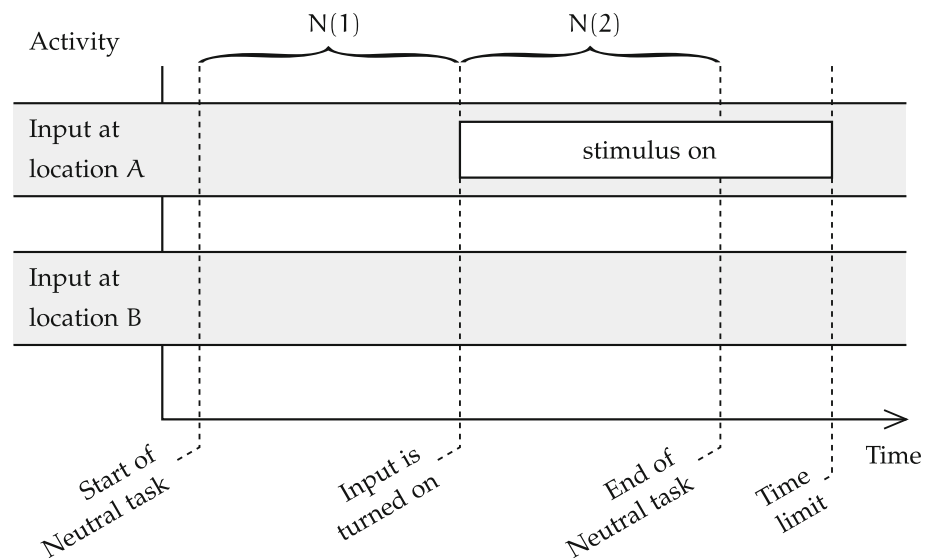
Fig. 2 Organisation of the Gap task condition in the simulated reflex attention shift experiment
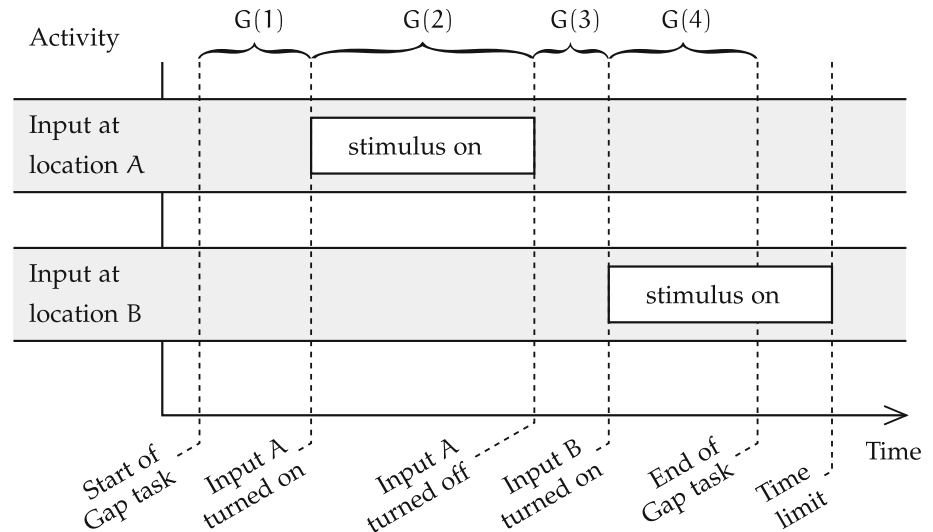
In this condition, neurons start at rest, and should remain so during phase $G(1)$, for the same reasons as in the Neutral condition. Similarly, during phase $G(2)$, output maps are expected to converge to the correct spatial and categorical activations to reflect the input presented at A, and sustain that activity until phase $G(3)$. Once input activity ceases at the start of phase $G(3)$, the network's overall activity is expected to gradually decrease, until phase $G(4)$. During phase $G(4)$, input is expected to drive the emergence of a different pair of outputs than during $G(2)$. However, the remaining activity from past input A may temporarily hinder convergence to category and spatial output representations of input B. Furthermore, the accommodation and hysteresis changes driven by channelopathy should affect that convergence delay. This effect of the model of channelopathy are of primary interest.

The overlap condition

The Overlap condition, shown in Fig. 3 is the second task meant to capture an attention shift process. In this task, the target appears while the distractor is still present.

Phases $O(1)$ and $O(2)$ of the Overlap condition are the same as $G(1)$ and $G(2)$ in the Gap condition. However, phase $O(3)$ consists in the simultaneous display on the input map of the first stimulus at location A, and of a second stimulus at a different location B. After a short while, in the last phase of the Overlap condition, the initial stimulus disappears, and the second stimulus remains displayed at location B [phase $O(4)$]. This last phase is finished when the output maps display the correct location and identity of the second stimulus. Like with other conditions, invalid outputs are those that have not converged to the correct identity and location within the imparted time. The total duration of phases $O(3)$ and $O(4)$ determines the

duration of reflex attention shift in the overlap condition, as the second stimulus appears at the start of $O(3)$.

The two first stages of the Overlap condition are the same as in the Gap condition; the same behaviour is expected. However, $O(3)$, in which two stimuli are simultaneously active at A and at B, is very different from $G(3)$, without input. Whereas overall activity should gradually decrease during $G(3)$, it should slightly increase in $O(3)$. Indeed, the goal of the Overlap condition is to examine reflex attention shift towards the new stimulus B in the presence of the existing detractor A. As the stimulus at A has already been displayed for the duration of $O(2)$ when $O(3)$ starts, the units that collectively represent it in each map of the spatial and object streams should be accommodated, allowing for the emergence of the representation of the new stimulus at B and the relative fading of that at A. Hence, during phase $O(4)$ with only the newer stimulus displayed, the attention shift may already be underway. As the effects of autism channelopathy on the tradeoff between focusing attention in one location and shifting attention to a new one are the main focus of the experiment, the effect of channelopathy on total attention shift time is measured. The emergent attention hypothesis implemented by unit accommodation and the dual-pathways vision model are the implementation context of this study of the focus/shift tradeoff; they are assumed sufficiently representative of the biological reality.

Model of channelopathy

There are two important mechanisms with respect to calcium channelopathy and visual attention. First, at the unit level, calcium channelopathy is assumed in the EVAC model to have behavioural consequences in autism. Second, the reflex visual attention processes are implemented

Fig. 3 Organisation of the Overlap task condition in the simulated reflex attention shift experiment
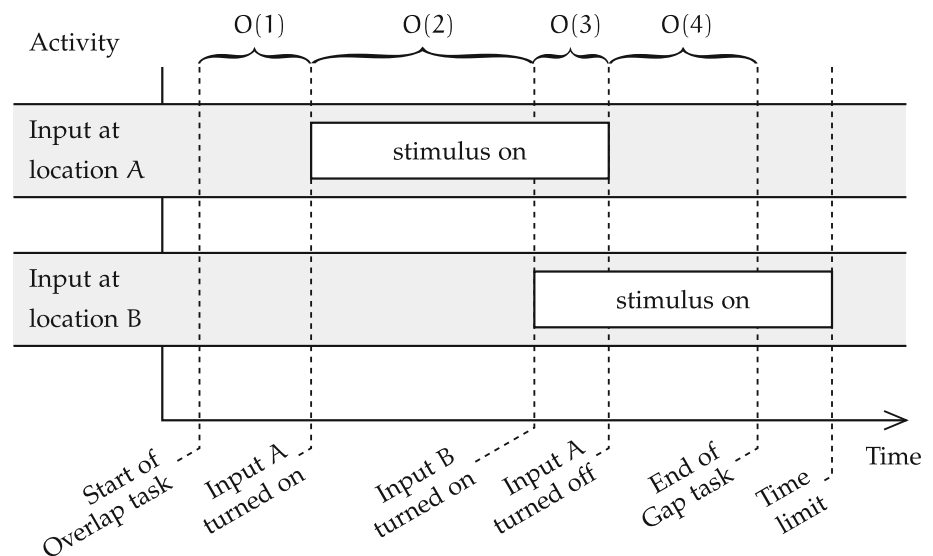
in EVAC both structurally, as the networks replicates visual streams, and at neuronal level, using unit accommodation as the main driver of reflex attention shift.

Calcium homeostasis and signalling in autism is a relatively unexplored topic in the literature. Existing studies hypothesised the emergent attentional effects of specific calcium channels defects as a possible root cause for some symptoms observed in cases of autism and autism spectrum disorders. They have indicated that calcium channelopathies may be common occurrences in autistic subjects (Lu et al. 2012; Gargus 2009).

There is evidence that disturbed immune activity during neurodevelopment may be part of the causal factors of autism, as the symptoms of autism have repeatedly led researchers to believe in a poorly regulated immune response of autistic children (Ashwood et al. 2006; Vargas et al. 2005). Such dysregulated immunity could impair the development of the neural system, as the latter depends on a balanced immune response (Ashwood et al. 2006). Furthermore, the maintenance of calcium homeostasis is crucially important in the functioning of immune cells,[3] and recent studies have revealed evidence of altered Ca^{2+} homeostasis in ASD (Palmieri et al. 2008; Napolioni et al. 2011). Together, these studies point towards a causal link

from channel-mediated intracellular calcium imbalance in autism and the disturbed neurodevelopment of autistic subjects.

There is also direct evidence of both offset calcium homeostasis and disturbed calcium signalling pathways in the autistic brain. Dysregulated calcium homeostasis has been observed at the macro level by Palmieri et al. (2008). This finding of dysregulated homeostasis was later linked with calcium signalling defects by Napolioni et al. (2011). It is known that voltage-gated calcium channels are essential to neuronal maturation and differentiation, in addition to their central function in neural information processing (McEnery et al. 1998). The body of evidence on these calcium signalling pathways anomalies in the neurons of autistic subjects consists primarily in a growing corpus of genetic studies. Indeed, the genetic evidence linking autism and calcium channelopathies is clear, as exposed by Gargus (2009). However, the exact nature of that link is not yet understood. Among recent works, (Lu et al. 2012) uses GWAS data to demonstrate that the calcium channel genes contributing to neuronal function have a definitive role in some cases of ASD.

The model of EVAC focuses on these potentially disturbed transmembrane calcium channels. One type of calcium channel, called voltage-gated calcium ion (Ca^{2+}) channel (VGCC), is of particular interest in neuronal dynamics. VGCC are very important actors in action potential (AP) propagation, in addition to being involved in muscular contraction, and endocrine and hormonal releases (Dolphin 2006). Their role in AP generation and propagation is cyclical, as it consists in further depolarisation of the membrane in response to an initial decrease of electrical potential. The modelled calcium channelopathy, which results in increased overall neural activation but

---

[3] Autistic subjects often suffer from a disturbed immune system (Ashwood et al. 2006). In parallel, the importance of calcium homeostasis in the immune response is evidenced by the cytopathic effects of the Ca^{2+} homeostatic imbalance triggered by several viral infections, see for instance (Poggi et al. 1998; Zocchi et al. 1998; Cheshenko et al. 2003). Misra et al. (1999) also showed that beryllium toxicity is in part the result of altered Ca^{2+} metabolism in mononuclear phagocytes consequent to reversible opening of plasma membrane channels, which not only reveals the central role of calcium homeostasis in the immune system, but also that of membrane calcium channels in that process.

longer accommodation, is hypothesised to model the effect on neural activity of the VGCC anomalies conmorbid with autism. Specifically, our working hypothesis of channelopathy is primarily justified by the recent linkage of defects in a subtype of VGCC called L-type voltage-gated calcium channels (LTCC) with the Timothy syndrome, a well-known channelopathy. The Timothy syndrome is notable for being one of the rare monogenic channelopathy paradigms, and furthermore presents core autism as a major symptom (Gargus 2009). Notably, the Timothy syndrome is a condition proven to be caused by the mutation of a gene (CACNA1C) encoding a sub-unit of LTCC (Splawski et al. 2004), and as such is proven to be the root cause of an autism-causing voltage-gated calcium channelopathy. Furthermore, LTCC are of particular importance in a number of the biological systems and processes whose disruptions produce significant symptoms of autism. Hence, the disturbed neurodevelopment and more frequent immune and gut problems of autistic children gives relevance to the hypothesis that calcium signalling disturbances (Krey and Dolmetsch 2007) is an important component the etiology of the syndrome.

It is necessary to verify that the proposed model of channelopathy triggers the expected electrical behaviour of individual neurons. For that, we analysed various scenarios by adjusting the parameters of the unit model and observing the effects on the simulated electrophysiological timeline.

The dysfunctions of LTCC present in cases of autism lead to an excess of calcium influx (Piedras-Rentería et al. 2007). LTCC are the main actors of the chain reaction that generates action potentials. We can model the excess of calcium influx during AP generation by increasing $\bar{g}_e$ above its control value, resulting in an increased depolarisation of the membrane for the same input. On short term, the unit is more active, but on longer term, the hysteresis and accommodation mechanisms, being activated by intracellular calcium concentrations, are expected to modulate the activity of the unit earlier.[4]

Accommodation and hysteresis are each modelled by one ionic channel that can be seen as letting positive or (respectively) negative charges into the cell, although it is likely that the phenomena of hysteresis and accommodation in biological neurons involve more channels and other triggers.

Figure 4 illustrates the behaviour of the model neuron subject to the approximations of accommodation and hysteresis (control unit), as compared to channelopathic units. The *net input* on Fig. 4 traces the external stimulus send to

the unit, turned on from cycle 10 to 200; *membrane voltage* is the membrane potential, *net current* traces the transfer of electrical charges through the membrane, and *net output* shows the rate-coded cell output.

Figure 4 superposes the activation of the control unit (faded traces, $\bar{g}_e = 0.4$, $dt_{b_h,inc} = dt_{b_a,inc} = 0.01$) to the activation of the unit implementing the proposed ion channel disturbances (dark traces, $\bar{g}_e = 0.45, dt_{b_h,inc} = dt_{b_a,inc} = 0.03$). The authors could find no published studies that would quantify the change in electrical properties of channelopathic neurons. Consequently, the values of the disturbed ion channel parameters were determined heuristically, so that the qualitative behaviour corresponds to the expected raised maximal excitability, earlier hysteresis, delayed and longer accommodation that can be expected from their functions (Lipscombe 2002) as illustrated in Fig. 4. The net input, the membrane potential, the transfer of electrical charges through the membrane, and the rate-coded cell output are all traced twice, once for the control unit, and once for the channelopathic unit. We observe that the model of channelopathy triggers a higher net input, following the larger $\bar{g}_e$, and an increased output rate, expected result of the raised excitability. Hysteresis takes place much earlier, and the start of the accommodation is slightly delayed by the influence of the larger earlier activity that on the basis variable. Accommodation and hysteresis lasts longer than in the control unit. While the total depolarisation obtained after hysteresis is higher than in the control, the difference is entirely accounted for by the larger initial depolarisation, and the additional offset brought by hysteresis is the same. Similarly, the hyperpolarisation that results from accommodation is of the same amplitude as in the control case. The fact that the voltage offsets of hysteresis and accommodation do not vary with channelopathy is reasonable, because hysteresis and accommodation are the phenomenologically modelled effects of a variety of cell mechanisms that are not expected to make direct use of LTCC (O'Reilly and Munakata 2000).

Visual pathways

The structure of the neural network of EVAC is designed following current knowledge and theories of visual pathways and reflex visual attention.

The hypothesis that channelopathic neurons lead to cortical networks with dynamic properties that are symptomatic of ASD only constrains the properties of the neuron model, and not of the network. The choice of which cortical network to model remains up to us modellers. It is reasonable to choose to model a subsystem for which existing computational models are known to replicate the

---

[4] These changes in timings of accommodation and hysteresis are simulated by decreasing respectively $dt_{b_a,inc}$ and $dt_{b_h,inc}$, as explained in Eqs. 4 and 5.

Fig. 4 Trace of the activation of a single unit with accommodation and hysteresis. The traces in *faded lines* correspond to a unit with standard parameters, and in *saturated lines*, to a unit modelling a calcium channelopathy

LEGEND

Control unit		Channelopathic unit
	net output produced	
	net input (after applying weights)	
	net current produced by all channels	
	membrane voltage	
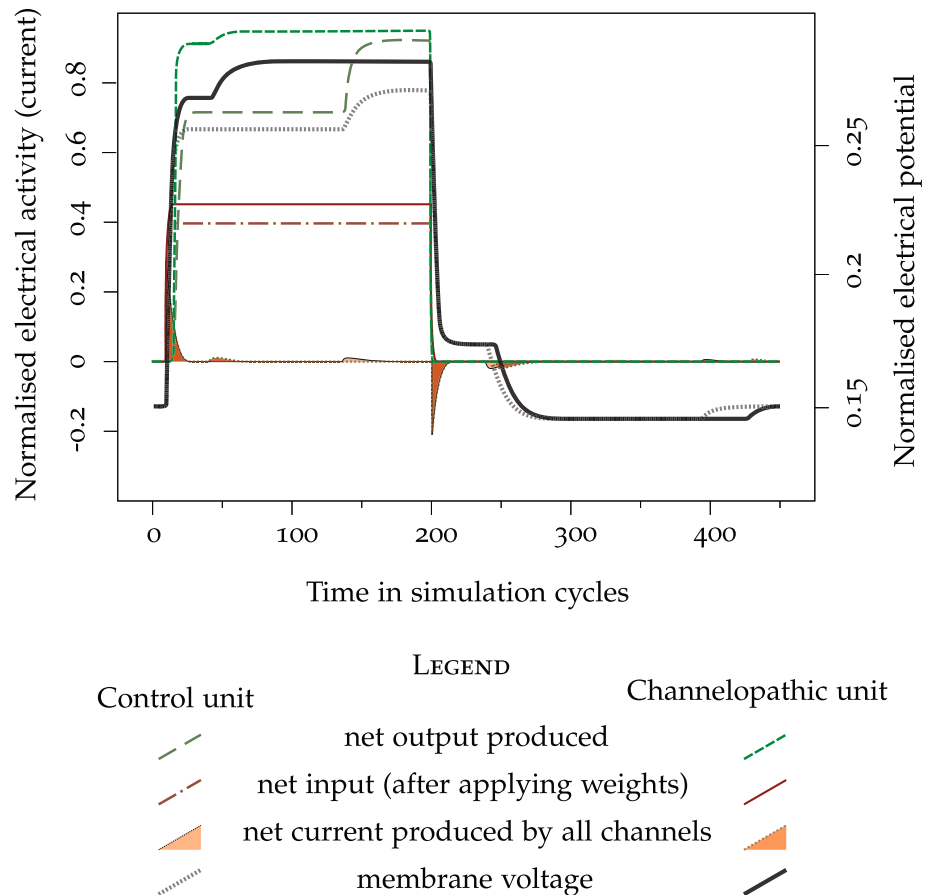
neural implementation with reasonable fidelity. Choosing a neural subsystem that is sufficiently well-understood is advantageous to build a simplified model with some understanding of the consequences of the simplifications made. In our case, we also want to have easily understood and experimentally accessible correspondences between the inputs and outputs of the model of EVAC and those observable in a similar psychological experiment on human subjects. To directly map model inputs to non-invasive experimental stimuli, the input layer of the model must correspond to a sensory area. Similarly, if one is to easily interpret the model response in terms of externally measurable behaviour, the output of EVAC should readily translate into expected muscular, physiological, or ERP[5] recordings.

Considering the above factors, we found that the reflex orientation of visual attention[6] seems an appropriate mechanism to model. Reflex attention designates the involuntary and fast focus of the abstract "attentional spotlight"[7] towards a stimulus. In the case of visual reflex attention, the focus is physiologically measurable by the orientation of the gaze, which occurs either by the saccadic rotation of the eyeballs alone or by the rotation of the head together with the compensated eye saccade. Hence, the output of a model of visual attention should translate into a physically measurable event. Input to the model is also sensory and well-understood. Furthermore, the mammalian visual systems are among the least misunderstood central nervous subsystems (Turiel and Parga 2003), and numerous computational models exist that accurately predict properties of the human visual system. Finally, several studies have revealed abnormal reflex orientation of visual attention in ASD subjects [see for instance (Elsabbagh et al. 2009; Geest et al. 2001; Townsend et al. 1996, 2001; Zwaigenbaum et al. 2005)]. Altogether, these properties make the study of the reflex orientation of attention in the visual system a prime candidate for the projection of the effects of calcium channelopathy on behaviour. In addition, there is a potential for generalisation of some results to

---

[5] Event-related potentials are EEG-recordable correlates of motor or cognitive events.

[6] Throughout this paper, reflex visual attention is also called bottom-up visual attention, visual attention capture, or, where there is no possible ambiguity, visual attention.

[7] The term "attentional spotlight" is mostly used to illustrate the selectivity of attention. It may not be a good illustration of the neurological processes underlying attention.

other modalities. First, the cortical networks are rather uniform in their microstructure. Second, primary sensory cortices share organisational features. So results obtained with a model of low-level visual attention may guide the explorations of aural, tactile or other modalities.

Overview of the visual system

In the human brain, visual information from one side of the visual field is processed by the contralateral hemisphere. Schematically, data are transmitted to successive cortical maps,[8] in a serial flow with recurrent modulatory connections.

The concept of *receptive field* of a neuron on a cortical map is central to the whole chain of visual processing. For a given neuron i receiving an input projection from an input map M, a receptive field of i on M is a set of topographically adjacent neurons of M that project their outputs on i. Figure 5 illustrates how each unit receives its input from a patch of topographically adjacent units of the preceding map.

This organisation results in an increasingly broader indirect coverage of the visual field by units farther along the processing chain. In Fig. 5, units are grouped into minicolumns, and sections of the input and post-synaptic maps with adjacent minicolumns are respectively denoted by A and B. Neuron j_1 in neural map B receives inputs from several adjacent units of the preceding layer A. Its neighbour, neuron j_2, is part of the same cortical minicolumn, and as such receives inputs from a similar set of neurons in A. All units in the minicolumn j have the same receptive field, and units from adjacent minicolumns share a portion of the receptive fields of their neighbours.

We follow Ungerleider and Haxby (1994), who schematise the organisation of the visual system using a dual pathway theory. The signal propagates from the retinas in the eyes, to the extrastriate cortices (V1 and V2), following the path of the optic nerves. These nerves start at the retina and transmit visual information to the optic chiasm, in which the nerve bundles are rearranged by hemisphere.[9] Then, the signals reach the LGN, which processes them to extract some microfeatures in both spatial and temporal domains. The processed signal is then transmitted to the primary visual cortex (V1), which performs further microfeatures extraction from several components of the visual signal using its receptive fields on the LGN. The same principles underlie the functioning of the secondary visual cortex (V2), which takes its inputs from the first visual cortex (V1), extracting slightly more complex features. After passing through V2, the visual

---

[8] Cortical map is the term used to name a sheet of cortical neurons with similar functions.

[9] This *decussation* of the optic nerves does not affect the information processing in EVAC.
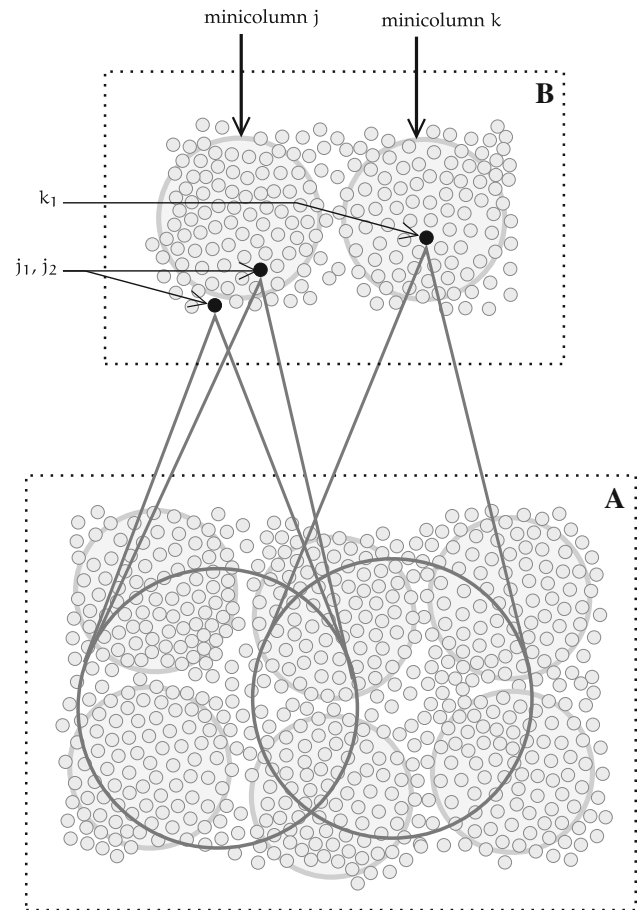
Fig. 5 Diagram illustrating the organisation of receptive fields (RF) in topographical cortical maps

pathway diverges into two separate streams, leading up to the splitting of the processing pathways into dorsal and ventral streams. The dorsal stream units are more sensitive to location information (position and motion), while the ventral stream units activate in response to the presence of geometric features of increasing complexity and with decreasing spatial location sensitivity. This *where-what duality* makes these two streams complementary. The ventral visual stream is considered to end in the inferior temporal cortex (IT), and the dorsal stream, in the posterior parietal cortex (PPT) (Ungerleider and Haxby 1994).

The EVAC model simplifies the biological pathways by only representing the identity of a simple visual stimulus (ventral pathway output) and its coarse spatial location (dorsal pathway output). It omits the more complex processing and interactions of later stages (Schenk and McIntosh 2010).

Each neural map of the visual system contains neurons that are each sensitive to one feature, but covering altogether the entire visual field with a wide variety of features. Most features are not absolute, but rather consist in local spatial or temporal differentials. In EVAC, we only tune

V1 neurons to the contrast orientation feature at a specific spatial frequency, because the input samples are unmoving black-and-white line drawings.

Neural unit model

Overview

The EVAC uses a point neuron model. The point neuron is a conductance-based model of biological neurons that abstracts the complex electrical state of the neuron into a vector of numbers aggregating the values of its ionic concentrations and trans-membrane ion flows. We choose this type of neuron model because it entails a level of abstraction that suits the goals of the model: the Hodgkin-Huxley equations used provide sufficient modelling power to represent channelopathy, while keeping the computational cost of the simulation manageable. The neuron model used comprises of five types of channels: the leak channel l, the excitatory input channel e, the inhibitory channel i, the accommodation channel a and the hysteresis channel h, in a system formalised and implemented by O'Reilly and Munakata (2000). For convenience, we use symbols similar to (O'Reilly and Munakata 2000).[10]

Three parameters model the state of each trans-membrane ionic channel α: E_α, g_α^t, and $\bar{g}_\alpha$.

Parameter E_α represents the reversal potential for the ion carried by channel α. This is the difference of electrical potential between the inside and the outside of the nerve cell at rest when the trans-membrane diffusion force of this ion is exactly countered by the electric force. The relative concentrations of ions on either side of the cytoplasmic membrane are considered constant because the currents are small and as biological mechanisms exist to maintain these concentrations. This first parameter is a static property of the cell.

Parameter g_α^t represent the proportion of the total number of channels α that are open.

Parameter $\bar{g}_\alpha$ indicates the total conductance for α when all of the channels for α are simultaneously open. The product $g_\alpha^t \bar{g}_\alpha$ consequently represents the conductance for channel α at time t.

At timestep t, the current I for some channel α is calculated using Ohm's law, as the conductance for that channel at t multiplied by the potential for that channel at t. The potential V_α^t for α at t depends on the membrane potential at t (V_m^t) and on the equilibrium potential of α denoted E_α; $V_\alpha^t = V_m^t - E_\alpha$. This gives Eq. 1:

$$I_\alpha^t = g_\alpha^t \bar{g}_\alpha \left(V_m^t - E_\alpha \right) \tag{1}$$

---

[10] In equations, literal symbols that relate to a particular channel are subscripted by a letter that identifies the channel, or by α for a generic expression applicable to several channels.

The above expression applies to all five α channels and thus models all ionic currents of the point neuron. It constitutes the basis to build the model of ionic current, and the dynamics of trans-membrane voltage. The following describes these five channels.

$\alpha = l$ The *leak* parameters model the constant potassium leak channels that the membrane of all neurons exhibits. The reversal potential of the leak channel is $E_l = 0.15$, its maximal conductance is $\bar{g}_l = 0.1$ and is always reached, so the proportion of open channels $g_l = 1$ at all times.

$\alpha = e$ The *excitatory* input synaptic channels let Na^+ enter the cell when glutamate released by the presynaptic cell binds to the synaptic receptor. Hence, the point unit model of the neuron lets g_e^t directly and linearly depends on the excitatory input, and is by definition within $[0, 1]$. g_e^t is therefore practically confounded with the unit's *net input*, as used in a traditional ANN. The arbitrary voltage and conductance units of the simulation are chosen such as $E_e = 1$ in the default case and $\bar{g}_e = 1$. The expression of the share of open excitatory input channels g_e^t is derived further below.

$\alpha = i$ The *inhibitory* channels are most often GABA-sensitive receptors that let Cl^- ions in to drive back the membrane potential towards the resting potential, as the reversal potential is the same as the membrane potential, $-70mV$ (0.15 in simulation units).

$\alpha = a$ Together with hysteresis (subscript h), *accommodation* allows the neuron to temporally integrate its state. The accommodation parameters are an abstraction of all ionic channels that are sensitive membrane potentials and ionic concentrations indicative of electrical activity, and which opening results in re-polarisation, and hence in inhibition. The mechanism of accommodation models neuronal fatigue. The default value of the resting potential $E_a = 0$ follows from the expected behaviour of accommodation to bring back the membrane potential to the resting value, while the value of $\bar{g}_a = \frac{1}{2}$ is empirically determined.

$\alpha = h$ *Hysteresis* is the reciprocal of accommodation: it designates the excitatory opening of channels in response to cell depolarisation, even in the absence of immediate synaptic input. This phenomenon does not conflict with accommodation because it operates on shorter time scales. The equations involved are formally the same, but the default dt_{b_h} parameter is larger than dt_{b_a}, resulting in the time scale differences observed *in vivo*.

For all channels, E_α and $\bar{g}_\alpha$ remain constant throughout each simulation. The leak channels do not adjust their opening rate, so typically $g_l^t = 1$. For other channels, g_α^t is variable. The precise update equation depends on the channel α considered, as ionic channels are sensitive to the different factors described above.

The functioning of ionic membrane channels approximation is shown for each type of channel (Eqs. 2–5).

Excitatory channel

Before giving the update equation of the excitatory input channel, it is necessary to describe the organisation of the unit inputs into *projections*. A projection consists in the conceptual grouping of inputs from the same cortical region. Projections are useful in EVAC because activity levels of inputs from different regions can greatly differ.

The excitatory conductance of the projection k (Eq. 2) is the the average of normalised inputs scaled to correct for expected activity α_k:

$$g_{e_k}^t = \frac{1}{\alpha_k} \langle x^t w \rangle_k \tag{2}$$

The total input to the unit is the average of the excitatory conductances of all n_p projections $\frac{1}{n_p} \sum_k g_{e_k}$. To update the excitatory conductance of the whole unit, an arbitrary term $dtnet \in]0,1[$ is used that scales g_e^{t+1} to a value between the previous value g_e^t and the net input. The effect of a unit bias weight term β that aggregates all differences in excitability that arise between any two neurons is integrated (O'Reilly and Munakata 2000).

The resulting expression (Eq. 3) updates the net input to a unit.

$$g_e^{t+1} = (1 - dt_{\text{net}})g_e^t + dt_{\text{net}}\left(\frac{1}{n_p}\sum_k g_{e_k}^{t+1} + \frac{\beta}{N}\right) \tag{3}$$

Accommodation and hysteresis

The update equation of the conductance of the accommodation and hysteresis channels have the same form, shown in Eq. 4:

$$g_\alpha^{t+1} = \begin{cases} g_\alpha^t + dt_{g_\alpha}\left(1 - g_\alpha^t\right) & \text{when} b_\alpha^{t+1} > \Theta_{\alpha,a} \\ g_\alpha^t + dt_{g_\alpha}\left(0 - g_\alpha^t\right) & \text{when} b_\alpha^{t+1} < \Theta_{\alpha,d} \end{cases} \tag{4}$$

where dt_{g_α} is a reactivity constant, and the variable b_α (introduced below) is compared to an activation threshold $\Theta_{\alpha,a}$ or a deactivation threshold $\Theta_{\alpha,d}$.

Equation 4 is hence naturally defined piece-wise, in terms of this estimate of recent unit activity b_α^t. b_α^t is

defined by Eq. 5:

$$b_\alpha^{t+1} = b_\alpha^t + dt_{b_\alpha}\left(y^{t+1} - b_\alpha^t\right) \tag{5}$$

where y^t is the rate-coded output of the unit, and the term dt_{b_α} adjusts the reactivity of b_α^t, hence reflecting how much time is integrated. The relatively longer setting delay of accommodation compared to hysteresis is implemented by varying the time integration parameters dt_{b_α} and dt_{g_α} present in Eqs. 4 and 5.

Inhibition

The inhibition of a unit is a function of the network structure because it integrates the recent activity of other units in the same neural map. Consequently, it is defined in "Modelling of lateral intra-map connectivity" section, after the network structure and connectivity has been. The numerical expression of g_i is shown in Eqs. 10 to 12.

Cell membrane current and voltage

Having determined how to compute all dynamic channels' conductances g_α, the current flow at the cell membrane I_α can be calculated at each timestep using Eq. 1.

From there, the trans-membrane electrical potential V_m is updated at each timestep following Eq. 6:

$$V_m^{t+1} = V_m^t - dt_{vm} \sum_{\alpha=e,i,l,a,h} I_\alpha^t \tag{6}$$

where dt_{vm} is a time-averaging parameter slowing down the change in membrane potential (O'Reilly and Munakata 2000) and I_α^t is the total electrical current going through the membrane at time t.

The integrate-and-fire mechanism of the neuron is modelled by Eq. 7 approximating the activation rate y^t.

$$y^t = \frac{\gamma\left[V_m^t - \Theta\right]_+}{\gamma\left[V_m^t - \Theta\right]_+ + 1} * \mathcal{N}\left(x, \frac{1}{200}\right) \tag{7}$$

where Θ is the membrane threshold for action potential generation, V_m^t is the trans-membrane electrical potential, and $\mathcal{N}\left(x, \frac{1}{200}\right)$ is a Gaussian noise kernel with variance 0.005. Equation 7 is the positive half of a sigmoïdal activation function with a gain parameter γ (defaulting to 600), like often encountered in artificial neural networks. In the present case, it is convoluted with a Gaussian function in order to better simulate the effects on instantaneous firing rate of the activation noise observed with live nerves. The parameter values have been determined by O'Reilly and Munakata (2000).

Network design, connectivity, and learning

Layer structure and connectivity

The architecture and processing mechanisms of the modelled network in EVAC aims at imitating some aspects of human visual pathways.

In reality, the human brain transmits richer visual signals and along more complex pathways. The EVAC model only retains those mechanisms essential for object-based reflex attention tasks. These mechanisms are based on the relevant biological visual pathways, following the general principles of cortical connectivity:

- afferent connections are accompanied by symmetrical efferent connections, effectively making networks recurrent (Sporns et al. 2007),
- the structure of maps and intra-map connectivity follow similar principles all across the cortex,
- inhibitory competition dynamics regulate intra-layer activity levels, and
- learning is implemented as a biologically plausible mix of Hebbian learning and two-phases error propagation.

The model of attention was build on previous simpler models of vision and of attention from O'Reilly and Munakata (2000). The connectivity follows the general principle of layered cortical maps with receptive fields (RF) connectivity and feedback. The units of each cortical layer are organised in cortical minicolumns, topographically adjacent ones covering adjacent regions in input space with some amount of RF overlap. Assuming a uniform distribution of input over the visual field, all the minicolumns of one layer can be set up to share a common set of weights.

The specific connectivity parameters and the general architecture of EVAC stem from the literature (O'Reilly and Munakata 2000). Figure 6 presents an overview of the network. The input layer accepts contrast images (in greyscale).

The input pattern is imposed onto a 48×48 input layer, from which lateral geniculate nucleus (LGN) units take their input. The LGN layer combines the processing of centre-surround ganglion cells of the retina and of the thalamus. This encoding enhances contrast areas of the input picture, letting cells of the first visual cortex (V1) respond to oriented edges with a polarity preference. V1 is an edge detector and is modelled by a 24×24 minicolumns map of 8 units per minicolumn, whose fixed weights form a set of Gabor filters that selectively respond to a specific orientation and polarity in the RF. Over the 8 units of each V1 minicolumns, 4 respond to edges oriented at 0°, 45°, 90° and 135° over RF of 6×6 on-centre LGN units, and the 4 other units of the V1 minicolumn respond
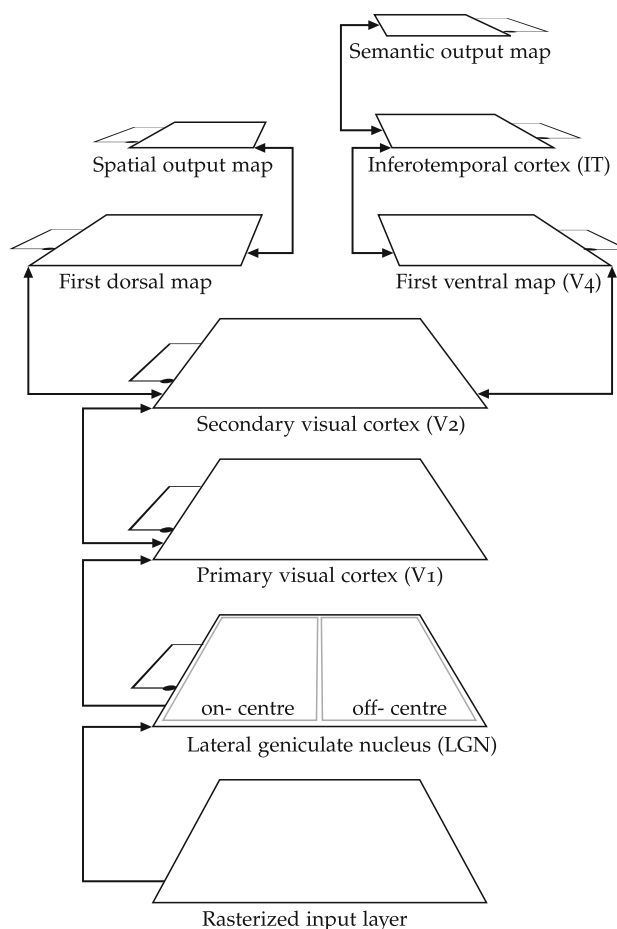
Fig. 6 Overview of the structure of the visual attention network

to the same angles, but over 6×6 RF of the off-centre LGN map.

V1 is connected to V2, a feature detector layer of 12×12 minicolumns. Each minicolumn contains 36 units with receptive fields of 16 V1 minicolumns. V2 cells respond to more complex features, while remaining spatially representative. The dorsal steam (left on Fig. 6) then specialises in responding to the spatial location of the stimulus, while the ventral stream (right) learns to respond to the category of the input.

V2 is connected to a simple ventral pathway starting with 6×6 minicolumns V4 map with 81 units per minicolumn. The RF of these minicolumns on V2 is 4×4 minicolumns with a 50 % overlap. The output of V4 is fully connected to a simple map of 12×12 units labelled IT, an intermediary representation which output is input of a semantic output layer. That output layer of 6 units is trained to associate one unit per object identity. It is meant to represents very roughly any higher level abstraction of the input (past the inferotemporal cortex); this abstract knowledge is learnt in a supervised manner, so as during the running phase, the semantic output layer shows the identity of the object.

Backward connections run back through both streams down to V1. Such feedback projections are also a typical pattern of connectivity throughout the cerebral cortex (Kandel et al. 1991). Backwards connectivity is omnipresent in the cortex; it is modelled here because it is assumed to be both a primary learning mechanism, used for the back-propagation of error signals, and to have a central role in the amplification of changes in relative activation due to neuronal fatigue.

All inter-layer connections are excitatory (arrowheads) and reciprocal starting from V1, letting higher layers influence feed-forward processing during learning and testing. All hidden and output layers recurrently inhibit themselves (k-WTA intra-layer inhibition), thereby regulating their own maximum activity levels.

All neural maps are typographically toroidal to avoid the effects of under-connectivity at the edge. Indeed, *in vivo*, networks are of much larger scale, and maps are regions of a continuous neural substrate. Consequently, edge effects are not observed and should be avoided in simulation.

Cortical networks structure

Cortical intra- and inter-map connectivity into logical layers is adapted from (O'Reilly and Munakata 2000).

Cortical maps are physically six-layered, and conceptually three-layered. The term "layer" will henceforth mean an abstract layer if not otherwise qualified. The input, hidden and output layers of a cortical map respectively correspond to physical layers 4, 2 and 3, 5 and 6. This *tiered organisation* is very consistent across the whole cortex, although the preponderance of each type of layer varies according to the use of the map.

The connectivity between and within layers of a cortical map is illustrated in Fig. 7.

The circular connectors represent inhibition, and the triangular ones are excitatory. Long-range cortical connections happen at physical layers 2 and 3. In the diagram, some abstract cortical regions *a*, *b* and *c* are chained into a processing pathway starting at input map *a*, passing through the "hidden" map *b*, and ending at output layer *c*. This shows how such structures integrate to form the connectivity between cortical regions.

Another principle of cortical networks is the *bidirectional character of map connectivity* (Kandel et al. 1991), hence the feedback connections from *b* to *a* and *c* to *b* on Fig. 7. This is a necessary condition for map development, as error-driven learning has to imply a form of error backpropagation, and a primordial mechanism of the regulation of reflex of visual attention.

Modelling of lateral intra-map connectivity

Within each map, the lateral connectivity is inhibitory on long neighbourhood range, and excitatory on shorter range. Lateral excitatory connections are represented by Gaussian-weighted connections to the topographical neighbours, while the more global inhibitory mechanisms are not explicitly modelled using inhibitory interneurons, but by the application of a map-level algorithm, the k-Winners-Take-All (k-WTA) inhibition scheme.

The k-WTA algorithm is directly derived from classical SOM learning algorithm, widely used in neural modelling (Kohonen 1982). In maps where units are functionally clustered in several minicolumns, the algorithm is applied twice. It is first applied among all units in a minicolumn and then to all units in a layer.

In its simplest form, the k-WTA function computes a common inhibitory channel opening g_i for all units of the map so that the k units with the highest excitatory input g_e are the only ones above threshold.

The expression of the inhibitory conductance at the threshold g_i^{Θ} in Eq. 8 is derived from Eq. 1:

$$g_i^{\Theta} = \frac{\overbrace{\sum_{\alpha \in \{l,a,h\}}^{\text{net current for l, a, and h}} (g_\alpha \bar{g}_\alpha (\Theta - E_\alpha)) + \overbrace{g_e^* \bar{g}_e (\Theta - E_\alpha)}^{\text{net excitatory current}}}^{I_{\text{net}}^t - I_i^t \text{ (without bias)}}}{\underbrace{E_i - \Theta}_{\text{potential between inhibitory equilibrium and AP threshold}}}$$

(8)

where Θ is a threshold membrane potential value, $g_i^{\Theta}(l)$ is the inhibitory conductance at the threshold Θ of unit l, which is the inhibitory conductance necessary to bring unit l to the AP-production threshold given its current excitatory input, and g_e^* is the excitatory input deprived from the bias input β (see Eq. 3).

From that point, two ways of computing the proportion of open inhibitory channels g_i are proposed:

– A simple mechanism consists in ordering units by their current level of excitatory input g_e and taking g_i between the inhibitory conductance at the threshold of unit k. Unit k is to be the weakest activated unit still included in the k winners, and unit $k + 1$, the strongest activated unit of the losers. A parameter q, defaulting to $\frac{1}{4}$, determines how close to $g_i^{\Theta}(k + 1)$ and $g_i^{\Theta}(k)$ the value of g_i is taken:

$$g_i = g_i^{\Theta}(k + 1) + q\big(g_i^{\Theta}(k) - g_i^{\Theta}(k + 1)\big) \tag{9}$$

– A more sophisticated calculation consists in taking the distributions of the top k units and of the remaining units by placing g_i between the respective averages of g_i^{Θ} for the top k units and bottom $N - k$ units, as in Eq. 10:

Fig. 7 Abstraction of cortical intra and inter-map connectivity [adapted from O'Reilly and Munakata (2000)]

The self-organised map (SOM) learning (Kohonen 1982) performed by EVAC extracts statistical correlations from the input patterns through re-normalised and contrast-enhanced Hebbian weights update. For hidden (non-clamped) units, once the net input has been computed, the k-WTA activation algorithm is applied. The weights from LGN to V1 are fixed so as each V1 unit responds to an oriented over its receptive field, and all unit or a V1 minicolumn are complementary in their coverage of orientations.

Weights between other layers are updated following the Leabra algorithm (O'Reilly 1996b), as a weighted combination of error-driven learning as per the Generalized Recirculation task learning rule and conditional principal components analysis (CPCA) model learning (O'Reilly and Munakata 2000) in the SOM context. Thus, for a unit indexed in its topological map by the subscripts i and j, Eq. 13 describing the weight update rule is obtained:

$$\Delta w_{ij} = \epsilon \left(k^{\text{hebb}} \Delta w_{ij}^{\text{hebb}} + \left(1 - k^{\text{hebb}} \right) \Delta w_{ij}^{\text{err}} \right) \tag{13}$$

where $\Delta w_{ij}^{\text{hebb}}$ is the associative learning of Eq. 15 and $\Delta w_{ij}^{\text{err}}$ is the error-driven change in weight defined in Eq. 18a. k^{hebb} controls the proportional influence of Hebbian association in total learning.

Oja's rule for Hebbian learning (Oja 1982) has been used to create learning algorithms that can be shown to converge to a representation of the principal components of the training set (Oja 1982). Oja' learning rule can be expressed as $\Delta w_{ij} = \epsilon\, y_j (x_i - y_j w_{ij})$, where i and j index respectively the pre-synaptic and post-synaptic units, and x and y denote input and output. O'Reilly and Munakata (2000) proposed a variation of Oja's rule that performs CPCA when used in presence of the inhibitory competition mechanics expounded in "Modelling of lateral intra-map connectivity" section.

The basic CPCA weight update is defined in Eq. 14:

$$g_i = \left\langle g_i^{\Theta} \right\rangle_{N-k} + q \left(\left\langle g_i^{\Theta} \right\rangle_k - \left\langle g_i^{\Theta} \right\rangle_{N-k} \right) \tag{10}$$

where the average of the inhibitory conductances at the threshold of the top k units is:

$$\left\langle g_i^{\Theta} \right\rangle_k = \frac{1}{k} \sum_{j=1}^{k} g_i^{\Theta}(j) \tag{11}$$

and for the bottom $N - k$ units:

$$\left\langle g_i^{\Theta} \right\rangle_{N-k} = \frac{1}{N-k} \sum_{j=k+1}^{N} g_i^{\Theta}(j) \tag{12}$$

The formulation in Eq. 10 is used in the model of EVAC.

Combined self-organised and error-driven learning

The learning algorithms set the weights of the synaptic connections so as the resulting pattern is likely to model the pattern of synaptic strengths in the corresponding areas in the brain.

In artificial neural networks, synaptic form often follows the details of the learning algorithm used. Thus, if we want the synaptic weights to form a network that is likely to reasonably model its cortical analogue, we have to employ a learning algorithm that mimics learning in the cortex. For that, we employ the Leabra algorithm, published by O'Reilly (1996b) and implemented in Emergent (O'Reilly and Munakata 2000). Additionally, the network is trained using a sure self-organising Hebbian association for features learning in the LGN-to-V1 projections.[11]

---

[11] The model's V1 minicolumns can be minimised into 8 units, covering 4 segments orientations and 2 polarities. In that case, LGN-to-V1 projection weights are not learnt but pre-defined. This is the case in the final implementation of EVAC.

$$\Delta w_{ij} = \epsilon\, y_j\left(x_i - w_{ij}\right) \tag{14}$$

The Hebbian learning rule in EVAC uses the CPCA weight update that is re-normalised by the sending layer's activity α shown in Eq. 15:

$$\Delta w_{ij}^{\text{hebb}} = \epsilon\left(y_i x_i\left(\frac{.5}{\alpha'} - w_{ij}\right) + y_j(1-x_i)\left(0 - w_{ij}\right)\right) \tag{15}$$

The parameter α' is a function of α, the expected layer activity level of the sending layer, of ϵ, a learning rate set heuristically, and of q, a parameter that balances the renormalisation of the layer:

$$\alpha' = \frac{1}{2} - q\left(\frac{1}{2} - \alpha\right) \tag{16}$$

when $q = 0$, Eq. 15 becomes the basic (not re-normalised) CPCA weight update equation.

With the Leabra algorithm, the learning of the hidden layers and output layers weights is aimed at being a biologically realistic mixture of Hebbian learning and error-driven learning (O'Reilly 1996b).

Error-driven learning is a fundamental problem in neural networks, and as such has been given numerous solutions, including the most notable back-propagation algorithm (Rumelhart et al. 1986).

Instead, the Emergent simulator offers a solution based on the Generalised Recirculation algorithm, or *GeneRec*, introduced in (Hinton and McClelland 1988). The GeneRec algorithm assumes that task learning involves two successive phases, "minus" and "plus". In the minus phase, the inputs are used to generate an expectation, as the output units run free. In the plus phase, both input and output units are clamped.

The supervised learning of GeneRec consists in modifying the weights according to the difference between the activations of the receiving units in each phase, proportionately to the average activation of the sending unit between the two phases (Eq. 17).

$$\Delta' w_{ij} = \epsilon\left(y_j^+ - y_j^-\right)\langle x_i\rangle_{-,+} \tag{17}$$

where y_j^+ represents the activation of the post-synaptic unit in the plus phase, and y_j^-, its output during the minus phase. $\langle x_i\rangle_{-,+}$ is the average activation of the pre-synaptic unit during the two phases. The learning rate constant ϵ is arbitrary and empirically chosen.

It can be shown that GeneRec approximates back-propagation (O'Reilly 1996a). This update mechanism is only valid when connectivity is roughly bidirectional and symmetric, so the average of the weight update in both directions is used to update the weights, leading to Eq. 18a, which corresponds to the update mechanism of the *Contrastive Hebbian Learning* (CHL) algorithm.

$$\Delta w_{ij}^{\text{err}} = \frac{\Delta' w_{ij} + \Delta' w_{ji}}{2} \tag{18a}$$

$$= \epsilon\left(x_i^+ y_j^+ - x_i^- y_j^-\right) \tag{18b}$$

Equation 18a is the task learning update rule. Together with the Hebbian model learning update rule of Eq. 15, they form the basis of the Leabra algorithm (O'Reilly 1996b), used in the model of EVAC to train the network weights.

Implementation framework

We decided to implement and run EVAC using the Emergent environment.[12] Emergent is the successor of PDP++, a piece of neural simulation software originally developed by McClelland and Rumelhart (1987).

One reason why Emergent is more appropriate for the implementation of the proposed model is that the reference book (O'Reilly and Munakata 2000) contains simplified models of emergent visual attention, on which EVAC is based. Although these models are much smaller in scale and do not feature accommodation-based reflex attention shifts, they provide a good basis for the incremental development of the larger-scale and more complex EVAC model.

In (O'Reilly and Munakata 2000), the authors also discussed a more complex model of visual attention which has been a source of inspiration for the EVAC model. However, this model of (O'Reilly and Munakata 2000) often fails to perform attention shifts from one object to the other, in what would be similar in their tasks models to the Overlap condition of EVAC.[13] The network structure is simpler, with a 2-layer spatial pathway connected laterally to V1 and V2. This model is implemented in PDP++, and has not been successfully ported to Emergent.

Emergent offers the possibility to work at the appropriate level of abstraction for the EVAC model of reflex attention. The neuron models are Hodgkin-Huxley point units and Emergent gives the possibility to add additional channels that model accommodation and hysteresis, mechanisms central to the EVAC model of attention shift.

The major drawback of using Emergent is its relative isolation from other modelling software. First, model description files are not implemented in or exportable to an open standard such as NeuroML or NineML. Second, an Emergent computational experiment is scripted in an esoteric language called C-Super-Script, used only by Emergent.

---

[12] Emergent version 5.0.2, 32 bit, available freely on Internet at grey.colourado.edu

[13] See authors' notes on their website at grey.colourado.edu/CompCogNeuro.

Despite these limitations, we have found that alternative software at the same level of abstraction do not cover our modelling needs, often by lack of appropriate neuron models to simulate accommodation and hysteresis. Thus, Emergent stands out as the most appropriate modelling and simulation environment for EVAC.

Statement of human and animal rights

This article does not contain any studies with human or animal subjects performed by the any of the authors.

Results

Statistical analysis

The network's response is measured in the three task conditions described in "Psychological tasks models" section: Neutral, Gap and Overlap. The Neutral condition measures the reaction time when the stimulus appears immediately after 50 time units without any stimulus. The Gap condition measures the reaction time when an interval of 50 time units separates the disappearance of the central stimulus and the appearance of the peripheral one. The Overlap condition measures the reaction time when the first stimulus remains visible during 50 time units after the second stimulus is displayed.

In these three conditions, maximal excitability, accommodation and hysteresis parameters are varied to simulate a channelopathy. As explained above, due to recent clinical studies of L-type voltage gated calcium channels (LTCC) and their role in the Timothy syndrome, L-type calcium channelopathy is hypothesised to result in increased calcium influx during action potential generation, and in increased overall neural activation but longer accommodation. In the model, the increases in maximal excitatory conductance and in the hysteresis and accommodation time integration constants correspond to these expected changes in calcium dynamics. The values of the parameters that vary between the two networks are as follows:

	$\bar{g}_e$	$dt_{b_h,inc}$	$dt_{b_a,inc}$
Control	0.4	0.01	0.01
Channelopathic	0.45	0.03	0.03

Each of the three task conditions of the experiment is repeated between 3900 and 4300 times per each of the two sets of parameter values. One parameter set corresponds to one group of subjects in the experimental setup. Invalid trials are defined as those with no response after 300 time units, or where the final spatial or semantic output mismatch the second stimulus. Such invalid trials are removed from all datasets.

The response time of the channelopathy-simulating (henceforth *channelopathic*) network is very different from that of the control network. This is first visible by the 10 % higher mean response time of the control network (58.3 vs 54.5 simulated time units). This difference in response time between the channelopathic and the control networks is dependent on the task. Indeed, on one hand, in the Neutral and Overlap conditions, the mean response time of the control network (57.5 and 86.7) is higher than that of the channelopathic network (52.4 and 73.7). On the other hand, the effect is reversed in the Gap condition, where the control network's response (33.5) is faster than the channelopathic network's response (37.2).

Additionally, the standard deviation of the response in the control network is much lower in the Gap task condition (σ in control: 4.23 (Gap), σ in channelopathy: 20.64 (Gap)), and a little higher in other conditions. There are more high-response time outliers in the response to the Gap condition in the channelopathic network.

To confidently determine whether the distributions underlying the reaction time of groups differ between one another, we attempt a two-way fixed-effects ANOVA. It allows us to reject the null hypothesis that the control and channelopathic networks timings datasets in each of the three task conditions are samples of the same population (p-values <0.001)

To further characterise these results, we fit a log-normal distribution to the data clustered by task condition $\times$ parameter set using MLE and report the results in Figs. 8, 9 and 10. Log-normal is a plausible distribution of clinical timing response, as left-bound experimental data is often found to be log-normally distributed Limpert et al. (2001), and in particular in reaction in times studies (Baayen and Milin 2010).

Each Figure 8, 9 and 10 corresponds to one task condition, and is organised by network type column-wise. For each task condition, each of the channelopathic and control networks parameter sets has been MLE-fitted to a log-normal distribution, and the parametric moments of reaction timing data are reported.

For parameter set a and condition b, the symbols $\hat{\mu}_{a,b}$ and $\hat{\sigma}_{a,b}$ denote the estimated location and scale parameters, which correspond to the mean and standard deviation of the logarithm of the timing values. Symbols $\mu_{a,b}$ and $\sigma_{a,b}$ refer to the arithmetic mean and standard deviation of the estimated log-normal distribution. Fitted trimmed histograms and quantile-quantile plots are shown in the bot-

Fig. 8 MLE-fitted log-normal distributions and parametric moments of reaction timing data for the Neutral condition

Neutral condition

Control parameter set		Channelopathic parameter set	
$\hat{\mu}_{ct,N} \approx 4.04959$	$\hat{\sigma}_{ct,N} \approx 0.06874$	$\hat{\mu}_{ch,N} \approx 3.9580$	$\hat{\sigma}_{ch,N} \approx 0.0594$
± 0.0010497	± 0.0007415	± 0.0009408	± 0.0006644
$\mu_{ct,N} \approx 57.51$	$\sigma_{ct,N} \approx 3.958$	$\mu_{ch,N} \approx 52.45$	$\sigma_{ch,N} \approx 3.122$
Range: $[44, 74]$	Gini: 0.03839	Range: $[42, 66]$	Gini: 0.03309
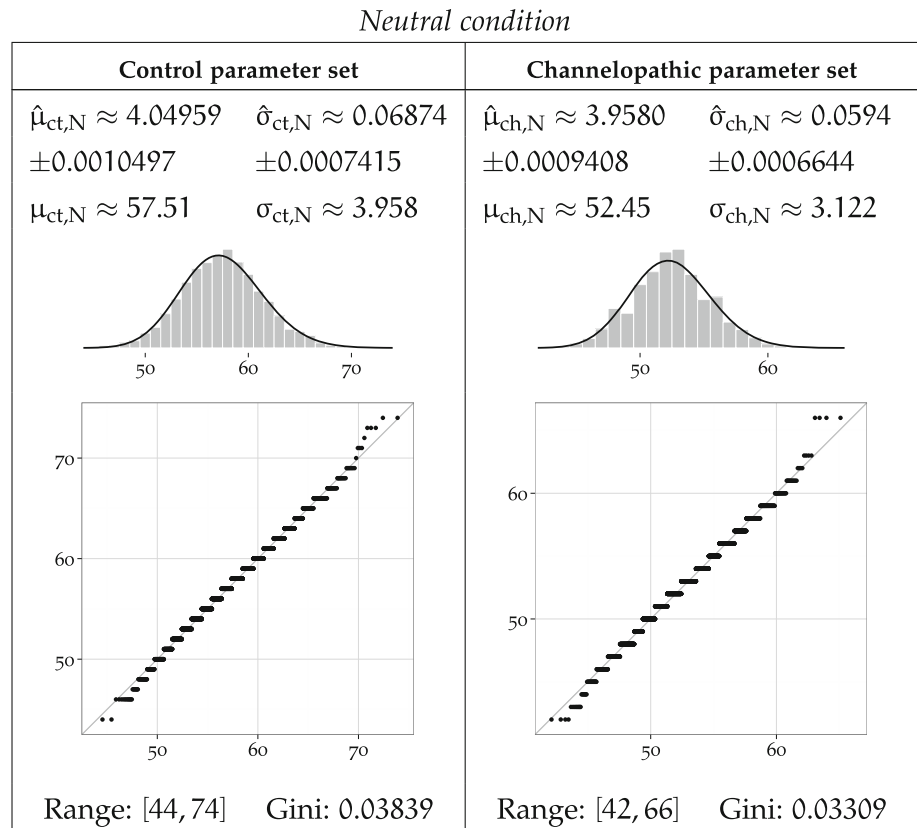
tom of each cell to illustrate the goodness of fit. The range of the dataset and the Gini coefficient are also reported to quantify statistical dispersion.

The theoretical probability density functions superposed to the density histograms in the Figs. 9 and 10 show a suboptimal fit, more pronounced for the channelopathic parameter set. For both network parameter sets, the log-normal distribution provides a good fit to the Neutral condition, but much less to the Overlap and Gap conditions. This is consistent with the heavy tails of the simulated data, which do not match their MLE-fitted log-normal hypotheses, as revealed by the quantile-quantile plots. The log-normal models are poor in that they do not always preserve the ordering of the datasets by variance.

It is notable that the Neutral condition does not exhibit this long tail on the right, and in both networks, the range of the data for that condition remains the lowest of all conditions.

In both networks, the Overlap task leads the longest mean reaction time, and the Gap task, to the shortest. The ordering of task conditions by performance (mean reaction time) does not vary between parameter sets. The Overlap condition is the slowest in both cases, followed by the Neutral condition, and ending with the Gap condition.

In the Overlap and Neutral task conditions, channelopathy facilitates attention shift, as it takes a longer mean time to shift attention for the control network than for the network modelling channelopathy, while in the Gap task condition, channelopathy hinders attention shift.

Sample standard deviation of the timing response in the control network is clearly lowest in the Neutral task, slightly higher in the Gap condition, and much higher for the Overlap. The Overlap condition has a higher standard deviation than the other, less demanding disengagement conditions.

The variance of the response delay to each task in channelopathic network is ordered differently from that of the control network. The Neutral condition also has the lowest variance, but the Overlap condition now takes the second place, and the Gap condition has the largest standard deviation.

The channelopathic network shows slightly less variance overall than the control network. The Neutral task follows that pattern, as channelopathy leads to slightly less variance than the control network. In the Overlap task, the control group timings are also a little more volatile. Finally, contrary to the Neutral and Overlap tasks, the standard deviations of the Gap task are very different

Fig. 9 MLE-fitted log-normal distributions and parametric moments of reaction timing data for the Gap condition

Range: $[15, 87]$ Gini: 0.06436 Range: $[25, 290]$ Gini: 0.1282
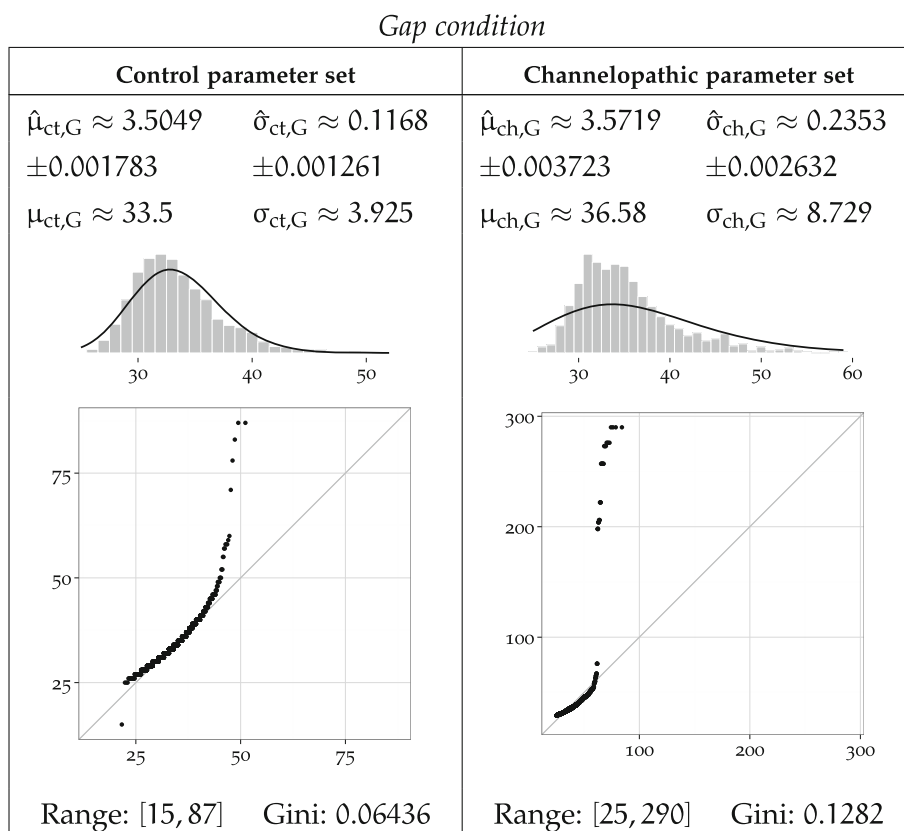
between network parameter sets, and are inverted: channelopathy leads to more variance.

Figures 8, 9 and 10 summarise the statistical properties of the response time of each network under each task condition. $\hat{\mu}_{net,C}$ and $\hat{\sigma}_{net,C}$ are the location an scale parameters of the log-normal distribution fitted to the response time data of network net on task C, with the 95 % confidence interval indicated below. $\mu_{net,C}$ and $\sigma_{net,C}$ are the sample mean and sample standard deviation. The histograms and quantile-quantile plots illustrate the fit of the log-normal distribution to the data.

Figures 8 to 10 illustrate that the ranges and dispersions of the groups differ. Timing output is more dispersed in attention switch tasks. The Neutral condition shows the lowest dispersion with both networks: the control × Neutral and channelopathy × Neutral groups have the lowest Gini coefficients among all groups. The output of these simulations are not as heavy right-tailed as others and their ranges are also the smallest. Without consideration of network type, the most dispersion between conditions is reached with the Overlap condition. However, contrary to the Neutral task, there is a large variation of range and/or dispersion between networks within both the Gap and and the Overlap conditions, hinting at a deep effect of the modelled channelopathy on attention shift. The effect is not the same between the two conditions: while channelopathy

in the Overlap condition does result in an increase in range span, the dispersion only changes by 9.8 %. In contrast, in the Gap task condition, both the response span and dispersion increase much with channelopathy. The log-normal distribution is much more a suitable model of the response time in the Neutral condition than in the Gap and Overlap tasks. This may reflect more complicated units interaction mechanics in the Gap and Overlap tasks as compared to the Neutral task.

Network performance

After presentation of the target input, for which the reaction time of the network is measured, the semantic layer is expected to output the class of the object presented within 300 time units. A trial is considered valid as soon as the corresponding identity unit is activated by more than 60 % of its maximum output rate.[14] When this expectation is not met, the trial is considered erroneous, and excluded from the response timing statistics.

---

[14] The 60 % threshold is arbitrary, but follows the convention of O'Reilly and Munakata (2000). Moreover, in the model of EVAC, the spurious activation of two or more semantic output units by more than 60 % each is made impossible by the use of a strict 1-WTA inhibition rule over the semantic output layer.

Fig. 10 MLE-fitted log-normal distributions and parametric moments of reaction timing data for the Overlap condition

Overlap condition

Control parameter set		Channelopathic parameter set	
$\hat{\mu}_{ct,O} \approx 4.4433$	$\hat{\sigma}_{ct,O} \approx 0.1883$	$\hat{\mu}_{ch,O} \approx 4.2818$	$\hat{\sigma}_{ch,O} \approx 0.1787$
± 0.003023	± 0.002137	± 0.002828	± 0.001999
$\mu_{ct,O} \approx 86.58$	$\sigma_{ct,O} \approx 16.45$	$\mu_{ch,O} \approx 73.53$	$\sigma_{ch,O} \approx 13.25$

Range: $[42, 223]$ Gini: 0.1056 Range: $[38, 240]$ Gini: 0.0952
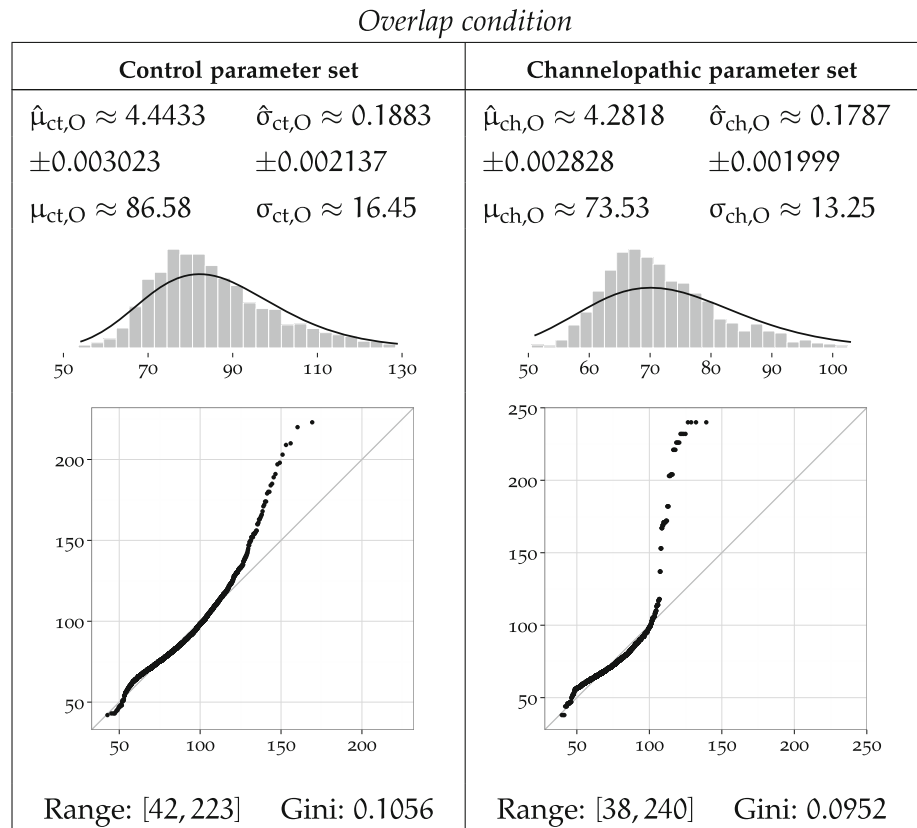
To complement the timing statistics on successful trials, the following section presents the performance of the trained network, calculated for each group (task × network) of N trials. Measures of network performance are r_ϵ for classification error rate and r_ζ for activation failure rate.[15]

The results are presented in Table 1, clustered by task condition and network.

The control network in Neutral condition outputs the correct class of the target unit within 300 time units in 100 % of cases. This is an expected result, as the control × Neutral group reflects both the training parameters and training inputs of the network: the training parameters are the same as the control parameters, except of course for the synaptic plasticity, with no influence on the independent dynamics of individual units. Also, like the target inputs of the Neutral task inputs, the training inputs are not preceded by a distractor.

This is unlike all other task × network groups, where either or both of the network type and task conditions differ

significantly from the training parameters and trial-level input sequences.

For each network type, the classification error rate remains consistently equal across all task conditions. For the control network, that is $r_{\zeta,ct} = 0$: spurious activation of an incorrect unit appears sufficiently unlikely not to be reflected in the datasets. The channelopathic network classification error rate is $r_{\zeta,ch} = 0.1\%$ in all tasks. This corresponds to exactly $N_{\zeta,ch} = 4$ incorrectly classified trials for each task group. This is a coincidence, and the 4 inputs that lead to the erroneous trials are not the same across tasks: the input table is a uniform random selection of symbol and retinal location that is different for each group (task condition × network), and the location, rotation and scaling parameters are continuously valued, making collisions very unlikely. Individual inspection of the inputs that triggered the classification errors shows that they all differ in location and identity.

The activation failures of the control network in attention shift tasks (particularly in Overlap) may be due to *incomplete attention shifts*. Contrary to the classification error rate, the activation failure rate is null in all channelopathy output datasets, and positive in control datasets. In the latter, the Gap task has a very low activation failure rate of $r_{\zeta,ct,G} \approx 0.047\%$, corresponding to $N_{\zeta,ct,G} = 2$ errors over $N_{ct,G} = 4288$ trials. This result contrasts with the high

---

[15] The classification error rate r_ϵ is $r_\epsilon = N_\epsilon/N$, where N_ϵ is the number trials where the wrong semantic output unit is activated by more than 0.6 in less than 301 time units. The activation failure rate r_ζ is defined by $r_\zeta = N_\zeta/N$ where N_ζ is the number of trials where no semantic output unit gets activated by more than 0.6 in less than 301 time units.

Table 1 Classification error rates and activation failure rates by network type (control, channelopathic) and task condition (Overlap, Neutral, Gap)

Task condition	Control		Channelopathy	
	Classification error rate	Activation failure rate	Classification error rate	Activation failure rate
All tasks	0	0.03179	0.001	0
Neutral	0	0	0.001	0
Gap	0	0.0004664	0.001	0
Overlap	0	0.09492	0.001	0

activation failure rate of the control network in the Overlap task condition: $r_{\zeta,ct,O} \approx 9.5\,\%$. In that case, most failures to activate the output unit above 0.6 come from a remarkable phenomenon: although the network state changes with the appearance of the target and further with the disappearance of the distractor, it reaches an equilibrium state in which enough activity correlated with the distractor is carried over after its disappearance to lead to a hybrid state where this spurious activity remains and prevents the complete transition to the target output. Typically, in that case, the semantic output units that correspond to the distractor and to the target both exhibit a low level of activity. Although we have no evidence that this network state is in any way similar to transitional states during successful attention shift in the Overlap condition, we deem it plausible, and call this type of phenomenon an *incomplete attention shift*. Formally defining and identifying it is not easy, because formalising incomplete attention shifts requires understanding the sparse distributed representations learnt by hidden layers in order to map the transition processes and be able to determine if a given snapshot of activity is part of a transition between two given inputs.

The systematic activation of the channelopathic network in all tasks ($r_{\zeta,ct} = 0$) indicates that such hypothesised "activation ties" are very unlikely to happen in this model in presence of channelopathy.

Due to recurrent dynamics, network activity slowly fades during the inter-stimulus pause of 50 cycles of the Gap task. The state of the network when the target appears is thus quite different from the Neutral case, which is only preceded by 50 cycles without input. Thus, a plausible explanation of the small activation failure rate of the control network in the Gap task is that it can also be prone to incomplete attention shifts.

Discussion

Having reviewed relevant studies on the psychology and neurology of autism, we determined that simulating the hypothetic effect on visual attention of channelopathies possibly linked to autism would be novel and significant.

We built a model of early dorsal and ventral visual pathways and their interactions for low-level attention, and implemented it in Emergent, along with learning and testing programs. The testing programs correspond to three tasks: two reflex attention shift tasks, and one simple attentional task that does not involve such attention shift. After implementing a phenomenological model of L-type voltage-gated calcium channelopathy, we verified that the cell model had the expected electrophysiological behaviour. We repeatedly ran the trained network on those three task and using either unit parameters simulating channelopathy or control unit parameters, collected a total of about 25,000 measures of response time and performance of the network. Finally, we used simple statistical tools to ensure that those response times differ significantly and to describe their empirical distributions. We quantified the classification error rate and activation failure rates of the networks for each group and qualified some note-worthy dynamics during activation failure in the overlap task of the network modelling channelopathy.

Model predictions

The EVAC model predicts the existence of a difference in the mean reaction time between gap and overlap conditions, such as the overlap condition is in average longer than the gap condition reaction time; this is a well-know occurrence of experimental psychology called the *gap effect*. It has been observed in close real-world equivalents to the simulated Gap and Overlap tasks conditions. The study by Saslow (1967) is an often-cited reference.

This result concords with the prediction of the EVAC model that the mean timing of the control network in the Gap task condition is significantly lower than in the Overlap condition. The concordance of the model with those experimental data about human gap effect is a comforting verification of its soundness.

EVAC makes several predictions about possible changes in the dynamics of attention shift in cases of disturbed accommodation and hysteresis. In hypothetical example, this may happen when voltage-gated calcium channels function atypically.

The Neutral task is used as a reference point relative to the two other tasks and models attention capture from a non-attentional state, while the Gap and Overlap tasks model reflex visual attention shift from recent and, respectively, concurrent current attentional engagement. The results are thus directly interpretable as predictions on the rates of classification error and of activation failure, and on the distribution of the reaction times in similar experiments involving biological neural networks. This includes experiments in psychology, if the measures performed can be commensurably related to the reaction of early visual streams modelled, and if the model of EVAC is sufficiently accurate despite its assumptions.

The most prominent prediction is that *current attentional engagement hinders attention shift* in both channelopathic and control subjects, as measured by the difference between the mean Overlap task timing and that of the Neutral task in both networks. The delaying effect of current attentional engagement measured in terms of ($\mu_O : \mu_N$) ratio—so, relative to the Neutral task—is larger in the control data (1.507) than in the channelopathic data (1.407). A relative measurement as ratio to the Neutral task is expected to be more robust to model simplifications than an attempt to get absolute timing predictions for direct comparison with clinical timing data. Indeed, the simulated experiment here is simplified in comparison to the reaction time study it intends to mimic. In particular, the reaction time in the real study would likely be measured using an indirect mean such as eye saccades, so the results would encompass the timing of motor activation as well. Even assuming that sufficient direct information about the attentional timeline of the neural maps involved is available, correspondence between the the absolute timings of the model response and of the human response seems unlikely, because the model of EVAC is not sufficiently faithful to the biological details.

In their clinical study of the reflex attention in autism, Geest et al. (2001) concluded that autism is correlated with a reduced gap effect. The prediction, drawn from the simulation of EVAC, that the relative negative effect of current attentional engagement on attention shift is less strong in channelopathy is thus concordant with the conclusions drawn in (Geest et al. 2001). The concordance of EVAC with this experiment is conclusive evidence in favour of the main theory of the model, under the premise that channelopathy is involved in the cases of the cited study.

The second prediction of the model is that *recent attentional engagement facilitates attention shift*. More precisely, this second prediction means that attention to a first stimulus followed by its removal for a short period, followed by the appearance of a distinct input stimulus, decreases the time required by the network to activate its representation of the second input stimulus. The ratios of the mean Gap timings to the Neutral timings are 0.5828 with the control network, and 0.7102 for the channelopathic network. In terms of the experimental psychology counterpart of the simulated experiment, this could mean that attentional capture from a completely blank field of view would take more time than attention shift in the Gap condition.

The third prediction of EVAC concerns the *spread of the timing responses* in each task. From the sample standard deviation of the groups in Figs. 8, 9, 10, variance is expected to be strongly increased by channelopathy in the Gap attention shift task $\left(\frac{s_{ch,G}}{s_{ct,G}} = 4.823\right)$, and slightly decreased in the Neutral and Overlap tasks $\left(\frac{s_{ch,N}}{s_{ct,N}} = 0.7885\right.$ and $\left.\frac{s_{ch,O}}{s_{ct,O}} = 0.9799\right)$. These predictions over dispersion are quite fragile, because the sources of noise included in EVAC are insufficient to accurately represent the plethora of sources of that variability are intrinsic to the biological system modelled.

The next group of predictions of EVAC relates to the *activation and success rates*. While those can be legitimately used to make predictions about the same rates in the biological equivalents of the neural systems modelled, it may prove harder to link the measured performance of the model to that of the subject in simple behavioural tasks in experimental psychology. The reason is that in EVAC, long-range top-down and sub-cortical inputs are ignored, but in reality, past the reflex saccadic movements of the eyes, other mechanisms exist that direct sight. It makes it unlikely that the inactive or erroneous steady state attained and maintained in the model in some proportions for a few groups actually occur behaviourally, in clinical subjects. For instance, the EVAC model predicts the occurrence of incomplete attention shifts in control subjects, most likely in activation failures of the Overlap task. Such error states would probably not be present in the form of steady equilibria like in the model. Rather, states like the incorrect or incomplete attention shifts predicted in the EVAC model will be disturbed by the constant, adaptive cortical and sub-cortical inputs to the visual streams. In practical consequence, this means that the experimental psychologist looking for evidence of the predictions below should preferably find a way to record the state of the concerned populations of neurons as the tasks are administered; or, when in sole possession of timing records, irregularities in the response time shall be hypothesised to be due to low-level failure of the network like in the model, so as the likelihood of those hypotheses may be tested by the usual means of probabilities and statistics.

The model predicts that a channelopathic visual system is unlikely to fail to activate on any of the three tasks, but

has a constant 0.1 % classification error rate. In comparison, the visual streams of control subjects are predicted to only be highly unlikely to fail to activate on the Neutral task, but to have a classification error rate very close to 0 on all tasks. However, like for the reaction times, we expect such absolute activation failure and classification error rates to be scaled and/or offset, such that the clinical results only concord with the model results in relative, ordinal terms. For instance, as $r_{\zeta,\text{ct,N}} = 0$ while $r_{\zeta,\text{ch,N}} = 0.1\%$ (Table 1), the classification error rate of the control subjects on the Neutral task is predicted to be lower than that of the channelopathic subjects. Along the same lines,

- the control subjects' activation failure rate is predicted to be the lowest in the Neutral task, higher in the Gap task, and the highest in the Overlap task,
- in all three tasks, the control subjects' classification error rates should be lower than the channelopathic subjects',
- in both the Overlap and Gap tasks, the channelopathic subjects' activation failure rate is predicted to be lower than the control subjects'.

Limitations

The scale of the modelled pathways and the novelty of the theories implemented have made it necessary to strike numerous compromises between model simplicity and accuracy to the biological phenomena. As a conceptual model integrating two novel hypotheses—that of autism calcium channelopathy and that of accommodation-driven low-level attention shifts—the picture drawn is approximate in the scales of many of the parameters involved, for lack of published data. To compensate for this limitation, it may be worthwhile investigating the integration of Standard Regularisation Theory in the modelling framework, as advised by Satoh and Usui (2009).

More than the reduced scale of the model, the lack of long-range top-down and sub-cortical influences in the model of EVAC is among the most hampering simplifications. It puts a hard limit on the timing that is interpretable as biologically plausible, as only short duration reflexes involving the early visual areas are accounted for. Prefrontal and other external influences are not modelled. While this may be sufficient for the type of reflex attention studied here, this may limit the interpretability of clinical experimental results. Modelling the effect of the hypothesised LTC channelopathy on different aspects of cognition could help circumventing this limitation, by including different pathways and sub-cortical connections. For instance, current works on the role of the hippocampus on bottom-up visual processing are particularly relevant (Sato and Yamaguchi 2009; Haab et al. 2011). Sato and Yamaguchi (2009) model short-term object-place association, which involves holistic scene processing and may differ in autistic subject by virtue of the differing attractor dynamics that could characterise autistic cognition Duch et al. (2013).

Another limitation of the model lies at the methodological level. On one hand, the aim is to make some progress in understanding possible causes of autism, which is a *developmental* disorder with proven anomalies in the structure of the central nervous system. A key feature of autism lies in the disturbed formation of the microstructure and connectivity of the brain during growth. On the other hand, we make use of a *statically-built* neural network to study a hypothesised cause of autism by looking at short-term reaction times, without considerations of possible developmental anomalies. Indeed, the simulated network is disturbed at unit level by the means of changes in hysteresis and accommodation, but remains the same structurally in control and channelopathic cases. Two reasons justify that choice. The first reason is that structural anomalies that would be due to calcium channelopathies as hypothesised in ASD have not been studied. However, autism in general tends to be linked to such anomalies, and it can be supposed that they are found in channelopathic cases as well. A priori, the evidence of minicolumnar anomalies expounded in (Casanova et al. 2006) applies to the visual pathways. However, they are not applicable to the quite abstract level of detail of the model of EVAC. This constitutes the second reason why both networks share the same structure: we could not find studies showing consistent anomalies at a scale that would affect the principles of cortical connectivity upon which the model is built. That, in itself, reveals a limitation of EVAC: it is too abstract to account for differences in the structure of units or of networks between autistic and control subjects.

Contributions

The proposed model combines a network model of emergent reflex attention and a unit model of the effects of calcium channelopathy on neuronal dynamics. To our knowledge, it is the first network-level computational model of the calcium channelopathy theory of autism outlined in (Adams and Snutch 2007). This approach has the potential to significantly impact research on channelopathies in several respects. First, it demonstrates the utility of neurocomputational models of low-level hypotheses of autism in understanding potential interaction with higher levels of cognition, possibly up to the behavioural level—as is the case with reflex attention shift. Second, EVAC gives avenues of experimental research to try and explore the behavioural phenotype of

channelopathic individuals. Emergent processes are not intuitive, thus simulations can improve the interpretability of computational models of low-level theories of autism causation. These improvements are potentially helpful in the general effort towards understanding, and eventually curing autism.

The network model of attention in EVAC is also an improvement over existing models of emergent reflex attention. There are several possible models of visual attention, some of which are able to account for bottom-up attention shift. The emergent model of reflex visual attention used in EVAC most resembles the two models of attention presented in (O'Reilly and Munakata 2000), as it is build upon their principles. However, the model of EVAC constitutes an improvement in scale and complexity that allows for some clinical predictions.

References

Adams P, Snutch T (2007) Calcium channelopathies: voltage-gated calcium channels. Springer, Berlin

Aisa B, Mingus B, OReilly R (2008) The emergent neural modeling system. Neural Netw 21(8):1146–1152

Ashwood P, Wills S, Van de Water J (2006) The immune response in autism: a new frontier for autism research. J Leukoc Biol 80(1):1–15

Baayen RH, Milin P (2010) Analyzing reaction times. Int J Psychol Res 3(2):12–28

Bower JM, Beeman D (1998) The book of GENESIS: exploring realistic neural models with the general neural simulation system. Springer. http://www.genesis-sim.org/GENESIS/iBoG/index.html

Casanova MF, Kooten IAJ, Switala AE, Engeland H, Heinsen H, Steinbusch HWM, Hof PR, Trippe J, Stone J, Schmitz C (2006) Minicolumnar abnormalities in autism. Acta Neuropathol 112(3):287–303

Cheshenko N, Del Rosario B, Woda C, Marcellino D, Satlin LM, Herold BC (2003) Herpes simplex virus triggers activation of calcium-signaling pathways. J Cell Biol 163(2):283–293

Courchesne E, Townsend J, Akshoomoff NA, Saitoh O, Yeung-Courchesne R, Lincoln AJ, James HE, Haas RH, Schreibman L, Lau L (1994) Impairment in shifting attention in autistic and cerebellar patients. Behav Neurosci 108:848–865

Dobosz K, Duch W (2010) Understanding neurodynamical systems via fuzzy symbolic dynamics. Neural Netw 23:487–496

Dolphin AC (2006) A short history of voltage-gated calcium channels. Br J Pharmacol 147(Suppl 1):S56–S62

Duch W, Dobosz K (2011) Visualization for understanding of neurodynamical systems. Cogn Neurodyn 5:145–160

Duch W, Dobosz K, Mikoajewski D (2013) Autism and ADHD–two ends of the same spectrum? Lect Notes Comput Sci 8226:623–630

Elsabbagh M, Volein A, Holmboe K, Tucker L, Csibra G, Baron-Cohen S, Bolton P, Charman T, Baird G, Johnson M (2009) Visual orienting in the early broader autism phenotype: disengagement and facilitation. J Child Psychol Psychiatry 50(5):637–642

Gargus JJ (2009) Genetic calcium signaling abnormalities in the central nervous system: seizures, migraine, and autism. Ann N Y Acad Sci 1151(1):133–156

Grossberg S, Seidman D (2006) Neural dynamics of autistic behaviors: cognitive, emotional, and timing substrates. Psychol Rev 113(3):483–525

Gu Y, Liljenstrm H (2007) A neural network model of attention-modulated neurodynamics. Cogn Neurodyn 1(4):275–285

Haab L, Trenado C, Mariam M, Strauss DJ (2011) Neurofunctional model of large-scale correlates of selective attention governed by stimulus-novelty. Cogn Neurodyn 5(1):103–111

Hinton G, McClelland J (1988) Learning representations by recirculation. Neural information processing systems. Denver, CO, 1987, p 358

Hodgkin AL, Huxley AF (1952) A quantitative description of membrane current and its application to conduction and excitation in nerve. J Physiol 117(4):500–544

Kandel E, Schwartz J, Jessell T, Mack S, Dodd J (1991) Principles of neural science, 4th edn. Elsevier, New York

Kohonen T (1982) Self-organized formation of topologically correct feature maps. Biol Cybern 43(1):59–69

Krey JF, Dolmetsch RE (2007) Molecular mechanisms of autism: a possible role for Ca^{2+} signaling. Curr Opin Neurobiol 17(1):112–119

Lanyon LJ, Denham SL (2009) Modelling attention in individual cells leads to a system with realistic saccade behaviours. Cogn Neurodyn 3(3):223–242

Limpert E, Stahel WA, Abbt M (2001) Log-normal distributions across the sciences: keys and clues. Bioscience 51(5):341

Lipscombe D (2002) L-type calcium channels: highs and new lows. Circ Res 90(9):933–935

Lu ATH, Dai X, Martinez-Agosto JA, Cantor RM (2012) Support for calcium channel gene defects in autism spectrum disorders. Mol Autism 3(1):18

McClelland J, Rumelhart D (1987) Explorations in parallel distributed processing handbook. MIT Press, Cambridge

McEnery MW, Vance CL, Begg CM, Lee WL, Choi Y, Dubel SJ (1998) Differential expression and association of calcium channel subunits in development and disease. J Bioenerg Biomembr 30(4):409–418

Michael R, Ivan I, Dan L, Michael W (2014) The role of de novo mutations in the genetics of autism spectrum disorders. Nat Rev Genet 15:133–141. doi:10.1038/nn1611

Misra UK, Gawdi G, Pizzo SV, Lewis JG (1999) Exposure of cultured murine peritoneal macrophages to low concentrations of beryllium induces increases in intracellular calcium concentrations and stimulates dna synthesis. J Leukoc Biol 65(6):786–791

Napolioni V, Persico AM, Porcelli V, Palmieri L (2011) The mitochondrial aspartate/glutamate carrier AGC1 and calcium homeostasis: physiological links and abnormalities in autism. Mol Neurobiol 44(1):83–92

O'Reilly R (1996a) Biologically plausible error-driven learning using local activation differences: the generalized recirculation algorithm. Neural Comput 8(5):895–938

O'Reilly R (1996b) The leabra model of neural interactions and learning in the neocortex. PhD thesis, Carnegie Mellon University

O'Reilly R, Munakata Y (2000) Computational explorations in cognitive neuroscience. MIT Press, Cambridge

Oja E (1982) Simplified neuron model as a principal component analyzer. J Math Biol 15(3):267–273

Palmieri L, Papaleo V, Porcelli V, Scarcia P, Gaita L, Sacco R, Hager J, Rousseau F, Curatolo P, Manzi B, Militerni R, Bravaccio C,

Trillo S, Schneider C, Melmed R, Elia M, Lenti C, Saccani M, Pascucci T, Puglisi-Allegra S, Reichelt KL, Persico AM (2008) Altered calcium homeostasis in autism-spectrum disorders: evidence from biochemical and genetic studies of the mitochondrial aspartate/glutamate carrier AGC1. Mol Psychiatry 15(1):38–52

Piedras-Rentería ES, Barrett CF, Cao YQ, Tsien RW (2007) Voltage-gated calcium channels, calcium signaling, and channelopathies. In: Krebs J, Michalak M (eds) Calcium—a matter of life or death, vol 41. Elsevier, Amsterdam, pp 127–166

Poggi A, Rubartelli A, Zocchi MR (1998) Involvement of dihydropyridine-sensitive calcium channels in human dendritic cell function. competition by hiv-1 tat. J Biol Chem 273(13): 7205–7209

Posner MI (1980) Orienting of attention. Q J Exp Psychol 32(1):3–25

Rumelhart DE, Hinton GE, Williams RJ (1986) Learning representations by back-propagating errors. Nature 323(6088):533–536

Saslow MG (1967) Effects of components of displacement-step stimuli upon latency for saccadic eye movement. J Opt Soc Am 57(8):1024–1029

Sato Naoyuki, Yamaguchi Yoko (2009) Spatial-area selective retrieval of multiple objectplace associations in a hierarchical cognitive map formed by theta phase coding. Cogn Neurodyn 3(2):131–140

Satoh S, Usui S (2009) Engineering-approach accelerates computational understanding of V1V2 neural properties. Cogn Neurodyn 3(1):1–8

Schenk T, McIntosh RD (2010) Do we have independent visual streams for perception and action? Cogn Neurosci 1(1):52–62

Splawski I, Timothy KW, Sharpe LM, Decher N, Kumar P, Bloise R, Napolitano C, Schwartz PJ, Joseph RM, Condouris K, Tager-Flusberg H, Priori SG, Sanguinetti MC, Keating MT (2004) Cav1.2 calcium channel dysfunction causes a multisystem disorder including arrhythmia and autism. Cell 119(1):19–31

Sporns O, Honey CJ, Kötter R (2007) Identification and classification of hubs in brain networks. PLoS ONE 2(10):e1049

Townsend J, Harris NS, Couchesne E (1996) Visual attention abnormalities in autism: delayed orienting to location. J Int Neuropsychol Soc 2(6):541–550

Townsend J, Westerfield M, Leaver E, Makeig S, Jung T, Pierce K, Courchesne E (2001) Event-related brain response abnormalities in autism: evidence for impaired cerebello-frontal spatial attention networks. Cogn Brain Res 11(1):127–145

Turiel A, Parga N (2003) Role of statistical symmetries in sensory coding: an optimal scale invariant code for vision. J Physiol Paris 97(4–6):491–502

Ungerleider LG, Haxby JV (1994) 'what' and 'where' in the human brain. Curr Opin Neurobiol 4(2):157–165

van der Geest JN, Kemner C, Camfferman G, Verbaten MN, van Engeland H (2001) Eye movements, visual attention, and autism: a saccadic reaction time study using the gap and overlap paradigm. Biol Psychiatry 50(8):614–619

Vargas DL, Nascimbene C, Krishnan C, Zimmerman AW, Pardo CA (2005) Neuroglial activation and neuroinflammation in the brain of patients with autism. Ann Neurol 57(1):67–81

Wany M, Wojcik GMN (2014) Shifting spatial attention—numerical model of posner experiment. Neurocomputing 135C:139–144

Zimmerman A (ed) (2008) Autism: current theories and evidence. Humana Press, New York

Zocchi MR, Rubartelli A, Morgavi P, Poggi A (1998) Hiv-1 tat inhibits human natural killer cell function by blocking l-type calcium channels. J Immunol 161(6):2938–2943

Zwaigenbaum L, Bryson S, Rogers T, Roberts W, Brian J, Szatmari P (2005) Behavioral manifestations of autism in the first year of life. Int J Dev Neurosci 23(2–3):143–152